




Solving the time-dependent Klein-Gordon and square-root Klein-Gordon equations with Krylov-subspace methods

Lei Geng ¹, Hao Liang ¹, Zi-Yang Lin ², and Liang-You Peng ^{1,3,4,5,*}

¹*State Key Laboratory for Mesoscopic Physics and Frontiers Science Center for Nano-optoelectronics, School of Physics, Peking University, 100871 Beijing, China*

²*School of Physics and Center of High Energy Physics, Peking University, Beijing 100871, China*

³*Collaborative Innovation Center of Quantum Matter, Beijing 100871, China*

⁴*Collaborative Innovation Center of Extreme Optics, Shanxi University, 030006 Taiyuan, China*

⁵*Beijing Academy of Quantum Information Sciences, Beijing 100193, China*



(Received 28 February 2023; revised 25 April 2023; accepted 15 May 2023; published 30 May 2023)

For relativistic spinless particles, the standard equation with Lorentz covariance is the Klein-Gordon equation, while the square-root Klein-Gordon equation, which is usually referred to be semirelativistic since it lacks Lorentz covariance, is another frequently used equation. We numerically solve these two equations coupled with time-dependent electromagnetic fields using the non-Hermitian Arnoldi and the Hermitian Lanczos propagator, respectively, in the three-dimensional real space. The non-Hermitian Arnoldi method is shown to be ideally suited for the Klein-Gordon equation. A different method to treat the nonlocal operator in the square-root Klein-Gordon equation is developed, allowing the calculation of the propagator to be more efficient. Furthermore, some strong-field problems such as the photoionization, high harmonic generation, and the pair production are studied using our methods. The results of both equations are compared with those of the nonrelativistic Schrödinger equation, which demonstrates the relativistic effects in various regimes. We show that observables of the Klein-Gordon equation and the square-root Klein-Gordon equation are identical up to the first order of relativistic corrections and confirm it numerically.

DOI: [10.1103/PhysRevA.107.053115](https://doi.org/10.1103/PhysRevA.107.053115)

I. INTRODUCTION

In relativistic quantum mechanics, the equations typically need to be covariant under the Lorentz transformation. So, the Schrödinger equation (SE) is replaced by the Klein-Gordon equation (KGE) and the Dirac equation for spin-0 and spin- $\frac{1}{2}$ particles, respectively. Additionally, there is also a simplified Klein-Gordon equation known as the square-root Klein-Gordon equation (SKGE). It is derived from the KGE's square-root form. Like the SE, it only includes the first derivative of time. Because of this, it uses less computational power while doing the time-dependent propagation numerically. Although it is not Lorentz covariant when the electromagnetic interaction is included [1] and the corresponding Hamiltonian is nonlocal. There still exist some hints that it does describe some physics for a relativistic problem [2,3]. The treatment based on this equation is known as semirelativistic. The comparison of full relativistic equations with semirelativistic ones is an important point in this paper. The results will show problems of SKGE do not prevent the equation to be a good alternative to the KGE in most conditions. The equation that only accounts for the leading-order correction of the SKGE is also referred to as the semirelativistic Schrödinger equation (SSE) in some references [4]. However, it has spurious solutions sometimes. We will show the distinctions

and connections of all these relativistic and semirelativistic equations in this article. The analytical properties of all the equations have been discussed thoroughly in the past [3,5]. But, it is still necessary to develop numerical methods to solve the equations, especially for time-dependent and non-perturbative problems, such as the photoionization, the high harmonic generation (HHG), and the pair production. For example, the three-dimensional time-dependent Dirac equations have been solved to study the photoionization process [6–9]. Without regard to the spin, the two-dimensional time-dependent KGE can also be used to investigate the interaction of laser and matter [10,11] as well as the pair production process [12]. In addition, the one-dimensional SKGE [13], the two-dimensional SSE [14], and the three-dimensional SSE [4,15,16] have also been used to study the relativistic effects of photoionization or HHG.

The solutions of time-dependent equations in full dimensions consume huge computational resources. So many researchers preferred to solve the equations in one or two dimensions. The soft-core Coulomb potential was used in this situation to avoid the Coulomb singularity. According to Ref. [17], this will lead to the improper description for the high-energy scattering cross section, which is important in the relativistic situation. In this work, we solve both the time-dependent KGE and SKGE in the three-dimensional spherical coordinates. The wave function is expanded in terms of spherical harmonics for the azimuthal coordinates, and the finite-element discrete variable representation (FE-DVR)

*liangyou.peng@pku.edu.cn

[18] is used to discretize the radial coordinate. The Coulomb singularity can be dealt properly in this scheme (please see Appendix A for details). Two types of propagators based on the Krylov-subspace methods are applied for these two equations, respectively, where both of them can be efficiently parallelized. For the KGE, the non-Hermitian Arnoldi propagator without the splitting operator is used, this method is shown to be more efficient and stable compared with the previous splitting scheme [10,19]. For the SKGE, we use the splitting operator to separate the kinetic and the potential energy operators of the Hamiltonian. A new Krylov subspace is defined for the kinetic part and the propagator of the nonlocal kinetic operator can be approximately solved in this subspace. The spurious solutions emerged in the SSE are absent in this case. Implementing all the numerical methods mentioned above, we test our schemes of these two equations by calculating bound eigenstates, photoionization, and HHG spectra. All the physical observables that are not related to the pair production in two equations are shown to be identical up to α^2 order from both analytical and numerical points of view.

The paper is organized as follows. In Sec. II, we give a brief introduction of the KGE in the Feshbach-Villars representation, followed by the description of its eigenstates and the propagation scheme. In Sec. III, we summarize the distinctions and connections between KGE, SKGE, and SSE, interspersing with some details about the numerical implementation. Then the propagation scheme of the SKGE is demonstrated. Section IV shows the numerical results of our programs and in Sec. V we give a short conclusion. Atomic units are employed throughout this article unless otherwise stated, where $c = 137.035999139$ a.u. is the speed of light.

II. KLEIN-GORDON EQUATION

In this section, we first introduce a commonly used representation, the Feshbach-Villars representation for the KGE. The Hamiltonian in the representation is shown to be pseudo-Hermitian. As a result, the charge conservation is preserved. Then, the method for numerically solving bound states and the analytical expression of scattering states are demonstrated. In order to compute the photoelectron momentum spectra, the amplitude of the projection is also given. The differences between the SE and the KGE on these points are discussed. At last, we introduce the non-Hermitian Arnoldi propagation scheme employed for KGE in our program. It is shown to have some advantages compared with the splitting operator scheme used in literature.

A. Klein-Gordon equation in the Feshbach-Villars representation

The KGE appears as a relativistic generalization of the SE in history. Although there were some difficulties to interpret the negative probability at the beginning, it was ultimately shown to be the correct relativistic equation for spin-0 particles [20]. Considering a particle with charge $q = -1$ and rest mass m_0 in the external field with scalar potential $\phi(\mathbf{r}, t)$ and vector potential $\mathbf{A}(\mathbf{r}, t)$, supposing $q\phi(\mathbf{r}, t) = V(\mathbf{r}, t)$, the equation can be written as

$$[i\partial_t - V(\mathbf{r}, t)]^2 \psi = \{[-i\nabla + \mathbf{A}(\mathbf{r}, t)]^2 c^2 + m_0^2 c^4\} \psi. \quad (1)$$

Different from the SE, the density of the particle is given by

$$\rho(\mathbf{r}, t) = \frac{1}{m_0 c^2} [\text{Im} \psi(\mathbf{r}, t) \partial_t \psi^*(\mathbf{r}, t) - V(\mathbf{r}, t) \psi(\mathbf{r}, t) \psi^*(\mathbf{r}, t)], \quad (2)$$

the possible negative value of density can be interpreted as the density of antiparticles. It is challenging to calculate the time-dependent propagation numerically in a direct manner since the equation incorporates the second derivative of time. In many cases, the standard KGE can be converted into another form named Feshbach-Villars representation [10,21], which has the same form as the SE,

$$i\partial_t \Psi = \hat{H} \Psi, \quad (3)$$

by redefining the Hamiltonian and the wave function. There is only the first derivative of time remaining in the equation since the other derivative is absorbed into the new two-component wave function Ψ . The relationship between the new and the old one is

$$\Psi = \begin{pmatrix} \Psi_1(\mathbf{r}, t) \\ \Psi_2(\mathbf{r}, t) \end{pmatrix} = \frac{1}{2} \begin{pmatrix} \psi(\mathbf{r}, t) + \frac{1}{m_0 c^2} [i\partial_t - V(\mathbf{r}, t)] \psi(\mathbf{r}, t) \\ \psi(\mathbf{r}, t) - \frac{1}{m_0 c^2} [i\partial_t - V(\mathbf{r}, t)] \psi(\mathbf{r}, t) \end{pmatrix}. \quad (4)$$

And the new Hamiltonian \hat{H} is a 2×2 matrix, with the form of

$$\hat{H} = [-i\nabla + \mathbf{A}(\mathbf{r}, t)]^2 \begin{pmatrix} 1 & \\ & -1 \end{pmatrix} + m_0 c^2 \eta + V(\mathbf{r}, t) \mathbf{I}, \quad (5)$$

in which \mathbf{I} is the 2×2 identical matrix and η is defined by

$$\eta = \begin{pmatrix} 1 & 0 \\ 0 & -1 \end{pmatrix}. \quad (6)$$

In this representation, the charge density can be expressed as

$$\rho(\mathbf{r}, t) = |\Psi_1(\mathbf{r}, t)|^2 - |\Psi_2(\mathbf{r}, t)|^2 = \Psi^\dagger(\mathbf{r}, t) \eta \Psi(\mathbf{r}, t). \quad (7)$$

It is evident that the new Hamiltonian \hat{H} is not Hermitian due to the nondiagonal terms, as a result, the corresponding propagator for Ψ is not unitary. However, the Hermitian conjugate of \hat{H} has the following relation with itself:

$$\hat{H}^\dagger = \eta \hat{H} \eta^{-1}, \quad (8)$$

which represents the pseudo-Hermiticity of the Hamiltonian [22–24]. As a consequence, the corresponding propagator \hat{U} is pseudounitary, satisfying

$$\hat{U}^\dagger = \eta \hat{U}^{-1} \eta^{-1}. \quad (9)$$

This guarantees that the total charge Q conserves even if it exists the pair production process:

$$\begin{aligned} \frac{dQ}{dt} &= \frac{d}{dt} \int \rho(\mathbf{r}, t) d\mathbf{r} = \frac{d}{dt} \int \Psi^\dagger(\mathbf{r}, t) \eta \Psi(\mathbf{r}, t) d\mathbf{r} \\ &= i \int \Psi^\dagger(\mathbf{r}, t) (\hat{H}^\dagger \eta - \eta \hat{H}) \Psi(\mathbf{r}, t) d\mathbf{r} = 0. \end{aligned} \quad (10)$$

B. Bound states and scattering states

Eigenstates are significant in the theoretical analysis because they contain the information about the behavior of

particles in the potential. It continues to be crucial in our numerical calculations. Taking photoionization as an example, the particle is excited from the bound state to the scattering state by a laser pulse. Therefore, it is crucial to compute both bound states used as the initial state and scattering states used for projecting at the end. Various methods are employed in the time-dependent Schrödinger equation (TDSE) program to accomplish this. The restarted Lanczos method [25] and the imaginary-time propagation method [26] are common approaches for solving bound states. The minimum solution method [27,28] and the Killingbeck-Miller method [29,30] are typical procedures for calculating the scattering states.

Let us focus on bound states first. The situation with the KGE is slightly different from that of the SE. Because the KGE contains both positive- and negative-energy states, the eigenvalues of the lowest few bound states that we want to solve exactly locate in the midst of all the states. Both the imaginary-time propagation method and the standard restarted Lanczos method aim to solve several eigenstates with minimal or maximum eigenvalues, which is not appropriate for this situation. We must look for alternative strategies. The exact diagonalization, which resolves all of the eigenvalues and eigenstates at once, is a simple and brute method. Although it may take a longer time than the procedures mentioned above and cannot be easily done in parallel computation, the consuming time is within the acceptable range. This treatment has been taken to get the initial state previously [16,31]. We use the subroutine DGEEV in the linear algebra package (LAPACK) [32] to complete this procedure.

The scattering state is what we focus on next. Different from the bound states, the scattering states are continuous in energy and nonlocal in the real space. In order to avoid the effect of the outside boundary condition in the coordinate r , they are usually given analytically or solved numerically from $r = 0$. For the Coulomb potential used in this work, it is easy to give the expression of scattering states analytically under both nonrelativistic conditions and relativistic conditions [5,33,34]. The Coulomb scattering wave function for a given wave number k and an angular quantum number ℓ in nonrelativistic conditions has the form [33]

$$\psi_{k\ell}(r) = \frac{e^{\pi Z/2k} |\Gamma(\ell + 1 - iZ/k)|}{(2\ell + 1)!} e^{-ikr} (2kr)^{\ell+1} \times F(\ell + 1 + iZ/k, 2\ell + 2, 2ikr), \quad (11)$$

where Z is the nuclear charge and F represents the confluent hypergeometric function. For the relativistic condition, the scattering state is in a similar form. By introducing $\gamma = \sqrt{(\ell + 1/2)^2 - Z^2/c^2}$ and $\mu = ZE/m_0c^2k$, the relativistic scattering state can now be written as [5,34]

$$\psi_{k\ell}(r) = \sqrt{\frac{E}{m_0c^2}} \frac{e^{\pi\mu/2} |\Gamma(\gamma + 1/2 - i\mu)|}{\Gamma(2\gamma)} e^{-ikr} (2kr)^{\gamma+1/2} \times F(\gamma + 1/2 + i\mu, 2\gamma + 1, 2ikr). \quad (12)$$

Note that E and k satisfy the relativistic dispersion relation $E^2 = k^2c^2 + m_0^2c^4$. It is necessary to stress that we take the normalization that is per unit charge in per unit length. As a result of Eq. (2), there is an additional $\sqrt{E/m_0c^2}$ factor in Eq. (12) in comparison to Eq. (11), which can also be clearly

understood via relativistic space contracts. In our program, we use the subroutine KLEIN [35] to calculate scattering states (12) with high accuracy.

To evaluate the photoionization cross section, the final wave function has to be projected to scattering states after the laser pulse turns off. For the SE, the amplitude for the momentum \mathbf{k} can be written as [36]

$$M_S(\mathbf{k}) = \frac{1}{\sqrt{2\pi k}} \sum_{\ell,m} e^{i(\delta_\ell - \ell\pi/2)} Y_{\ell m}(\hat{\mathbf{k}}) \times \int_0^\infty \psi_{\text{final},\ell m}(r) \psi_{k\ell}(r) r^2 dr, \quad (13)$$

where $Y_{\ell m}$ are the spherical harmonics. For the KGE, due to the pseudo-Hermiticity of the Hamiltonian in the Feshbach-Villars representation, the pseudometric η should be inserted in the integral

$$M_{\text{KG}}(\mathbf{k}) = \frac{1}{\sqrt{2\pi k}} \sum_{\ell,m} e^{i(\delta_\ell - \ell\pi/2)} Y_{\ell m}(\hat{\mathbf{k}}) \times \int_0^\infty \Psi_{\text{final},\ell m}(r) \eta \Psi_{k\ell}(r) r^2 dr. \quad (14)$$

As we can see from Eqs. (11) and (12), the Coulomb phase shifts δ_ℓ are also different in the two situations. It equals $\arg \Gamma(\ell + 1 - iZ/k)$ and $\arg \Gamma(\gamma + 1/2 - i\mu)$ for Eqs. (13) and (14), respectively. The relativistic corrections of scattering states and phase shifts we discuss here are usually missed in past works.

C. Arnoldi propagation scheme

Krylov-subspace methods are a class of algorithms for solving linear algebra problems, in which the best-known ones are Arnoldi and Lanczos methods [37]. Their key idea is searching for an approximate solution in the Krylov subspace by doing the matrix-vector product iteratively. This characteristic makes it easy to be parallelized because the matrix-vector product can be done in blocks easily for different cores on a cluster. Additionally, for the sparse matrix that frequently appears in physical problems, the matrix-vector product calculation requires far less effort. Thus, the Krylov-subspace approach has emerged as one of the most significant computational physics algorithms. We use the Krylov-subspace method to evolve the time-dependent propagation of the wave function. The eigenvalues of the Hamiltonian matrix need to be solved based on a set of orthogonal vectors in the Krylov subspace. In the SE, the evolution of the wave function ψ in a short time δt can be expressed as

$$\psi(t + \delta t) = e^{-i\hat{H}\delta t} \psi(t) = \left(1 - i\hat{H}\delta t - \frac{1}{2}\hat{H}^2\delta t^2 \dots\right) \psi(t). \quad (15)$$

It is clear that the wave function $\psi(t + \delta t)$ lies within the space spanned by $\{\hat{H}^n \psi | n \in \mathbb{N}\}$. For a small time step δt , it is mainly contributed by the first few vectors. And the error of the propagator $e^{-i\hat{H}\delta t}$ can be controlled within a bound if the series n is truncated from 0 to $N - 1$ [38]. The space spanned by the vector sequence is known as the Krylov subspace of N

order:

$$K_N = \text{span}(\psi, \hat{H}\psi, \hat{H}^2\psi, \dots, \hat{H}^{N-1}\psi). \quad (16)$$

It should be noted that the vectors above are not orthogonal; we can use the modified Gram-Schmidt process to generate a sequence of orthonormal vectors q_0, q_1, \dots, q_{N-1} . After that, the Hamiltonian can be represented in this set of basis $h_{ij} = \langle q_i | H | q_j \rangle$, which is a $N \times N$ upper-Hessenberg matrix. This procedure is called the Arnoldi iteration. Particularly, the matrix is a tridiagonal matrix when the Hamiltonian is Hermitian and the procedure reduces to the Lanczos algorithm. The matrix h_{ij} can then be diagonalized using the QR matrix decomposition in LAPACK:

$$S^{-1}hS = E = \begin{pmatrix} E_0 & & & \\ & \ddots & & \\ & & \ddots & \\ & & & E_{N-1} \end{pmatrix}. \quad (17)$$

Now, the evolution of the wave function in a short time can be expressed by the sequence of vector q_n [39]

$$\begin{aligned} \psi(t + \delta t) &= e^{-i\hat{H}\delta t} \psi(t) \\ &= (q_0 \quad q_1 \quad \dots \quad q_{N-1}) S e^{-iE\delta t} S^{-1} \begin{pmatrix} 1 \\ 0 \\ \vdots \\ 0 \end{pmatrix}. \end{aligned} \quad (18)$$

As mentioned above, the KGE can be written in the form of the SE. Therefore, Eq. (18) also can be used to calculate the time-dependent evolution of wave function for Eq. (3). The Arnoldi propagator should be utilized because the Hamiltonian (5) is non-Hermitian. This situation is different from the TDSE with the exterior complex scaling [39], in which the wave function is absorbed from a distance and the norm of the wave function decreases. In our case, the norm (not the charge) of the wave function Ψ increases. This implies that the eigenvalues E_n contain the positive imaginary parts. Theoretically, the numerical error can be exponentially magnified for an eigenvalue with a significantly positive imaginary part. Nevertheless, our calculations do not show such instability. It may be explained by the comparatively modest imaginary part of eigenvalues E_n for all the major wave-function components. The Arnoldi algorithm performs surprisingly well in this case. Bearing in mind that this is not the only origin of errors, the Krylov subspace is truncated up to a finite order of N for each time step. So there must be a small amount of wave function omitted in the subspace, which is deserted in our calculations. Despite all of these, the charge of the wave function is still conserved with very high accuracy. We will show the concrete value in Sec. IV D. Not all the schemes perform well on this problem; we also test the non-Hermitian Lanczos method [40] in our case, but it crashes quickly for the time propagation.

There exists another scheme to propagate the KGE based on the splitting operator method. As in Refs. [10,11], the Hamiltonian can be separated into two parts

$$\begin{aligned} H_1 &= V(\mathbf{r}, t)\mathbf{I} + m_0c^2\eta, \\ H_2 &= [-i\nabla + \mathbf{A}(\mathbf{r}, t)]^2 \begin{pmatrix} 1 & \\ & -1 \end{pmatrix}. \end{aligned} \quad (19)$$

The propagator can be approximated as

$$\begin{aligned} U(t, t + \delta t) &= \exp(-iH\delta t) \\ &\approx \exp(-iH_1\delta t/2) \exp(-iH_2\delta t) \exp(-iH_1\delta t/2) \\ &\approx \exp(-iH_1\delta t/2) (1 - iH_2\delta t) \exp(-iH_1\delta t/2). \end{aligned} \quad (20)$$

The propagator of the Hamiltonian H_2 is simplified in this way. Because the matrix H_2 is nilpotent, the high-order terms in its propagator are all zeros. But the method also introduces errors, the splitting operator method origins from the well-known Baker-Campbell-Hausdorff formula, which is

$$\begin{aligned} e^X e^Y &= e^Z, \quad Z = X + Y + \frac{1}{2}[X, Y] \\ &\quad + \frac{1}{12}[X - Y, [X, Y]] + \dots, \end{aligned} \quad (21)$$

where the square brackets represent the commutator. We would get the splitting operator method by picking the expansion of the leading order. The error of the method comes from the higher-order terms, which is due to the noncommutativity of the operators H_1 and H_2 . It is easy to check that $[H_1, H_2] \sim \nabla^2 V(\mathbf{r}, t) - i\nabla V \cdot \mathbf{A}(\mathbf{r}, t) + m_0c^2[-i\nabla + \mathbf{A}(\mathbf{r}, t)]^2$. The first two terms also appear in the splitting operator scheme of common TDSE and only cause minor errors. However, the last term is proportional to m_0c^2 . Thus, the time step has to be in a magnitude of $1/m_0c^2$ to keep the error within an acceptable range, which demands a high computational cost.

In our scheme, no splitting is used and all the Hamiltonians are contained in the Arnoldi iteration, which not only improves the precision, but also reduces the instability. The success of the Arnoldi algorithm in this case demonstrates the versatility and excellent precision of the method. In addition, the Arnoldi method has a lot of other advantages, such as accessibility and transplantability. One can easily implement it by some well-developed libraries like Arnoldi package (ARPACK) [41].

III. SQUARE-ROOT KLEIN-GORDON EQUATION

In this section, we first raise the SKGE from the KGE. The distinctions and connections between the two equations are demonstrated. The existence of the nonlocal square-root operator in SKGE is also addressed. For the Coulomb potential, the ground-state energies of two equations are shown to have the same first-order relativistic correction. We prove a relationship between the eigenstates of the two equations, which results in the fact that all the observables have the same first-order relativistic correction in the two equations. Next, we compare the SKGE with the commonly used SSE. It demonstrates that the difference between these two equations mainly lies in the high-order derivatives. So some numerical problems caused by high-order terms are discussed. At last, we present a propagation scheme employed for SKGE in our program. It calculates the square-root operator in a Krylov subspace and contains more components compared with the classical scheme.

A. Distinctions and connections between Klein-Gordon and square-root Klein-Gordon equations

We have introduced the KGE and associated algorithms in the previous section. Now let us discuss the other equation focused on in the article, which is the SKGE. Their similar names make it obvious that they are related. The expression of the SKGE

$$[i\partial_t - V(\mathbf{r}, t)]\psi(\mathbf{r}, t) = \sqrt{[-i\nabla + \mathbf{A}(\mathbf{r}, t)]^2 c^2 + m_0^2 c^4} \psi(\mathbf{r}, t) \quad (22)$$

is just like a square root of Eq. (1). Because it can also be derived from the Bethe-Salpeter formalism under some approximations, the equation is sometimes referred to as the one-particle spinless Salpeter equation [3]. The discrepancies between Eqs. (1) and (22) are usually overlooked mistakenly or purposefully in some studies. Clarifying the distinctions and connections between these relativistic and semirelativistic equations is one of the purposes of this work.

The main connection between the KGE and the SKGE is that they both share the relativistic dispersion relation, which is $E^2 = p^2 c^2 + m_0^2 c^4$. This suggests that they partially satisfy the special relativity. The distinctions between them are embodied in many aspects. For example, the SKGE is covariant only when there is no external field [1,42]. When the interaction with an electromagnetic field is taken into account, the SKGE does not admit the Lorentz group. This is the main reason why this equation is not widely used. Another obstacle that prevents its prevalence is the square-root operator. The operator is a pseudodifferential operator [43] rather than a common differential operator. The square-root operator in Eq. (22) can be understood as

$$\begin{aligned} & \sqrt{[-i\nabla + \mathbf{A}(\mathbf{r}, t)]^2 c^2 + m_0^2 c^4} \psi(\mathbf{r}, t) \\ &= \frac{1}{(2\pi)^3} \iint \sqrt{[\mathbf{p} + \mathbf{A}(\mathbf{r}', t)]^2 c^2 + m_0^2 c^4} \\ & \times e^{i[\mathbf{p} + \mathbf{A}(\mathbf{r}', t)] \cdot (\mathbf{r} - \mathbf{r}')} \psi(\mathbf{r}', t) d\mathbf{r}' d\mathbf{p}. \end{aligned} \quad (23)$$

The square-root operator is defined as the integral in the whole momentum and real space acted on the wave function. That means the wave function at one point can affect the propagation of wave function at any point in the domain through the integral. It becomes apparent that the square-root operator is a nonlocal operator in theory, which is in contrast to the common operator in the SE. This may lead to an infinite maximum speed, which would seem to go against the special relativity. But it is not in truth. It can be proven that the nonlocality does not disturb the light cone structure [43]. All the observables agree with the relativity principle. The conclusion is also verified numerically [44]. Nevertheless, such a nonlocal operator is intractable for numerical calculations. The matrix of the operator in the real-space representation is a dense matrix as opposed to a banded matrix. Therefore, most of the studies either concentrate on its analytical properties [42,45] or only simulate some simple cases [44,46] like the free Gaussian wave packet. Studies for more complicated situations where the Coulomb potential or the time-dependent external field involved is still rare. In this contribution, we will introduce an approximative algorithm to solve the time-dependent

propagation of wave function with the square-root operator using the Krylov subspace. Details will be provided in Sec. III C.

There are some other differences between the two equations. The SKGE only contains the first derivative of time and the positive-energy solutions in contrast to the KGE. So the issue of negative probability in the KGE is eliminated. In a sense, the SKGE is more like the SE rather than the KGE, just with the Hamiltonian $\sqrt{[-i\nabla + \mathbf{A}(\mathbf{r}, t)]^2 c^2 + m_0^2 c^4} + V(\mathbf{r}, t)$. The distinctions of KGE and the SKGE also can be reflected in their eigenvalues and eigenvectors. For the field-free $\mathbf{A}(\mathbf{r}, t) = 0$ case with an attractive Coulomb potential $V(\mathbf{r}, t) = -Z/r$, the Hamiltonian in Eq. (22) is also known as the Herbst Hamiltonian [47]. There do not exist analytic solutions to its eigenvalues, which has attracted some studies about its spectral property. The most important conclusion is that the Hamiltonian has discrete energy levels with the lower bound [47]

$$\sqrt{-\nabla^2 c^2 + m_0^2 c^4} - \frac{Z}{r} \geq m_0 c^2 \sqrt{1 - \left(\frac{\pi Z}{2c}\right)^2} \quad (24)$$

for the spectrum in $[0, m_0 c^2)$ when $Z \leq 2c/\pi$. This means the equation is more stable for a large nuclear charge compared with the KGE because the lowest eigenvalue of the latter becomes complex for $Z \geq c/2$ [5]. The perturbative properties of SKGE's eigenvalues and eigenvectors were also studied in some other works [48–50]. Taking the $1s$ state as an example, the eigenvalue's perturbative expansion has the form

$$E_0 = m_0 \left[c^2 - \frac{Z^2}{2} - \frac{5Z^4}{8c^2} + \frac{8Z^5}{3\pi c^3} + O\left(\frac{1}{c^4}\right) \right], \quad (25)$$

which deviates from the accurate result of the KGE

$$\begin{aligned} E_0 &= m_0 c^2 \left[1 + \left(\frac{Z}{c/2 + \sqrt{(c/2)^2 - Z^2}} \right)^2 \right]^{-1/2} \\ &= m_0 \left[c^2 - \frac{Z^2}{2} - \frac{5Z^4}{8c^2} - \frac{21Z^6}{16c^4} + O\left(\frac{1}{c^6}\right) \right], \end{aligned} \quad (26)$$

at the order of $1/c^3$ and higher. But they are identical up to the $1/c^2$ order, which is the leading order of the relativistic correction. Actually, the first-order relativistic corrections for SKGE and KGE are the same for all the observables except for the pair creation process, not only the eigenvalue. It could be demonstrated by the following relationship between their eigenvectors up to $O(1/c^2)$:

$$\begin{aligned} \psi_{S,E} &\approx \sqrt{\frac{E - V(r)}{m_0 c^2}} \psi_{KG,E} \\ &\approx \left[1 + \frac{E - m_0 c^2 - V(r)}{2m_0 c^2} \right] \psi_{KG,E}, \end{aligned} \quad (27)$$

where $\psi_{S,E}$ and $\psi_{KG,E}$ is the eigenstate of SKGE and KGE with eigenvalue E , respectively. Combining Eqs. (27) and (4), one can easily check the equation

$$\begin{aligned} \langle \Psi_{KG} | \hat{O} | \eta \Psi_{KG} \rangle &= \sum_i \sum_j \langle a_i \Psi_{KG,E_i} | \hat{O} | \eta a_j \Psi_{KG,E_j} \rangle \\ &\approx \sum_i \sum_j \langle a_i \psi_{S,E_i} | \hat{O} | a_j \psi_{S,E_j} \rangle \\ &= \langle \psi_S | \hat{O} | \psi_S \rangle \end{aligned} \quad (28)$$

holds for any observable \hat{O} up to $O(1/c^2)$. The complete proof for Eq. (27) is given in Appendix B. In addition, Eq. (27) is also confirmed numerically. We have described how to solve the eigenvectors for the KGE in Sec. II B. With respect to the eigenvectors of SKGE, we can solve it numerically using the method in Ref. [51]. Suppose the kinetic operator $\hat{O} = -\nabla^2 c^2 + m_0^2 c^4$ can be expressed as a matrix M in the Lagrange mesh, and it can be diagonalized by the similarity transformation $S^{-1}MS = E$. Then the corresponding square-root operator can be written as $\sqrt{\hat{O}} = S\sqrt{ES}^{-1}$. After that, we add the potential part and do the diagonalization again to generate the eigenvectors. Some bound states solved numerically for these two equations will be presented in Sec. IV A, demonstrating the great accuracy of Eq. (27). Using this relation, we can multiply a factor on the analytical scattering states of the KGE to approximate the scattering states of the SKGE, which does not have the analytical expression.

B. High-order derivatives in square-root Klein-Gordon equation compared with semirelativistic Schrödinger equation

Another commonly used semirelativistic equation is the SSE. Sometimes, people confuse it with the SKGE. Actually, they indeed have very close connections. The distinctions of them mainly embody in high-order derivatives. We will also drop in the problems caused by these terms in this subsection. Let us first concentrate on the SSE equation, which takes the form of

$$i\partial_t \psi = \left\{ \frac{[-i\nabla + A(\mathbf{r}, t)]^2}{2m_0} - \frac{[-i\nabla + A(\mathbf{r}, t)]^4}{8m_0^3 c^2} + V(\mathbf{r}, t) \right\} \psi. \quad (29)$$

There are a lot of ways to derive it. The simplest way is to expand the square-root operator of the SKGE in the Taylor series, then keep terms up to $O(1/c^2)$ order and omit the constant term $m_0 c^2$. Other ways involve diagonalizing the KGE up to the first-order relativistic correction with the help of the Foldy-Wouthuysen transformation [52] and ignoring the spin-related terms in the Breit equation. Overall, it has more connections than distinctions with the SKGE. They have the same Hamiltonian up to $O(1/c^2)$. And they are both in the form of the SE so that they have the same expression of charge density $\rho(\mathbf{r}, t) = \psi^*(\mathbf{r}, t)\psi(\mathbf{r}, t)$. All these shared characteristics make them perform almost identically in numerical calculations under most of the conditions.

The distinctions between them are also apparent. First, there does not exist a ground state for the Coulomb potential in Eq. (29) from an analytical point of view. In principle, the momentum could be arbitrarily large. Thus, the kinetic

energy $p^2/2m_0 - p^4/8m_0^3 c^2$ has no lower bound. But, in the real numerical calculation, we can still obtain a ground state with a less dense grid since such grids only support wave function with a finite momentum. However, the high-energy portion is typically significant in relativistic conditions. The dense grid is essential if one needs a precise solution. SSE performs badly in this condition. Unphysical eigenstates with negative energies and intense oscillations appear when we diagonalize its Hamiltonian. An example will be shown in Sec. IV A. In order to solve this issue, at least one more term $p^6/16m_0^5 c^4$ in the Taylor series should be taken into account for a lower bound of the Hamiltonian. As a result, more matrix multiplications have to be performed in this manner. In the following, we will concentrate on such high-order operators. So one may ask why this equation is used frequently in the relativistic problems [15,16] despite this drawback. This could be attributable to another distinction between the two equations. There is no nonlocal operator in the SSE, which makes it easier for the numerical calculation since one does not need to deal with a dense matrix. Additionally, it is a reliable approximation in most circumstances.

We have stated the differences between the two equations mainly lie in higher-order derivatives. Therefore, it is necessary to pay attention to the problems caused by high-order terms. The matrix expression of these terms is the first issue. In our program, operators are expressed as matrices once the equation has been numerically discretized. For the common Gauss-Lobatto quadrature, the matrices of the first derivative and the second derivative operators have been given in Appendix A. They are quite accurate despite the presence of the Coulomb singularity. The situation, however, is no longer true for higher-order derivatives. For example, the operator p^2 can be written as the matrix T :

$$\begin{aligned} T_{i,j} = \langle \psi | p^2 | \psi \rangle_{i,j} &= \int_0^{r_{\max}} \chi_i \frac{1}{r} \frac{d}{dr} r^2 \frac{d}{dr} \frac{1}{r} \chi_j dr \\ &= \int_0^{r_{\max}} \chi_i \frac{d^2}{dr^2} \chi_j dr \end{aligned} \quad (30)$$

with the boundary condition $\chi(0) = 0$. Note that the s state is considered here for simplicity since there is no centrifugal potential. But the matrix T^2 does not represent the operator p^4 if $\partial^2 \chi(0)/\partial r^2 \neq 0$,

$$\begin{aligned} \langle \psi | p^4 | \psi \rangle_{i,j} &= \int_0^{r_{\max}} \chi_i \frac{1}{r} \frac{d}{dr} r^2 \frac{d}{dr} \frac{1}{r} \frac{d}{dr} r^2 \frac{d}{dr} \frac{1}{r} \chi_j dr \\ &\neq \sum_k T_{i,k} T_{k,j}. \end{aligned} \quad (31)$$

Nevertheless, the deviation can be managed within a very small range. The error for the expectation of the operator is about $w_{1,1}[\partial^2 \chi(0)/\partial r^2]^2$, where $w_{1,1}$ is the weight of the first grid point. It goes to zero when the grid size decreases to zero or the wave function near the boundary $r = 0$ is sufficiently smooth. Another way to reduce the error is by seeking other numerical differential schemes. In the Gauss-Radau quadrature, using T^2 to represent the operator p^4 performs substantially better than the Gauss-Lobatto quadrature because it does not impose a constraint on the boundary value of the integral function. The concrete results

of these two configurations for different equations will be displayed in Sec. IV A. Although the grid discretization causes inevitable precision loss for the high-order derivatives, it is still possible to improve precision significantly by choosing appropriate numerical differential schemes for specific problems. Aside from the high-order derivatives themselves, other operators such as the propagator $e^{-i\hat{p}^2\delta t}$ and the Hamiltonian $\sqrt{p^2c^2 + m_0^2c^4}$ that can be expanded by series of p^2 also contain high-order derivatives. As a result, there always exist errors when we use the matrix T to represent the operator p^2 in these operators. For the nonrelativistic TDSE, the error only exists in the time-dependent propagation. In contrast, the error is directly reflected in the eigenvalues of the Coulomb potential for relativistic equations.

Another problem induced by the high-order derivatives is the wave-function boundary condition. For the SE without higher-order derivatives, it is believed that the wave function $\psi(\mathbf{r})$ has a finite value anywhere. That indicates the boundary condition is $\chi(0) = 0$. So the Gauss-Lobatto quadrature is usually employed in the first finite element and the value on its left end point is set to 0 in the common TDSE. When taking the relativistic effects into account, the wave-function correction $\Delta\chi(0)$ for the s state at $r = 0$ is not zero and even diverges, which is in conflict with the general assumption. The problem exists for all the relativistic and semirelativistic equations considered in this article. Technically, we should use the Gauss-Radau quadrature in the first finite element. Because the boundary condition for the Gauss-Radau quadrature is free so the wave function is permitted to be nonzero at $r = 0$. However, it has been demonstrated that the divergence of the wave function may cease at a length scale shorter than the electron Compton wavelength [53]. It will not cause significant effects for observables if the boundary condition $\chi(0) = 0$ is still used.

C. Splitting operator and square-root propagator in Krylov subspace

In the subsections above, all the topics for SKGE are discussed without imposing the laser field. Now, we will focus on how to propagate the SKGE in the presence of external fields in this subsection. Since the Hamiltonian is nonlocal in SKGE, as we said before, it makes it difficult to propagate the wave function accurately. However, the contributions from the first few Taylor expansion terms of the square-root operator dominate for the condition that is not too extreme. We can mainly consider these contributions. If the Hamiltonian is rewritten to retain the first few terms of relativistic corrections, a lot of matrix-vector multiplications need to be performed for calculating $H\psi$ in the standard Arnoldi iteration. To reduce the computation demand, a splitting operator method combined with Krylov-subspace method is proposed. It will be shown in the following.

The splitting operator method is usually used in the calculation of TDSE in order to dissociate the Hamiltonians in different spaces [10,54,55] or to reduce the stiffness of the problem [56]. It has been briefly introduced in Sec. II C. Since the Hamiltonian of SKGE contains two parts, i.e., $\sqrt{(-i\nabla + \mathbf{A})^2c^2 + m_0^2c^4}$ and V , the short-time propagator can

be written as

$$U(t, t + \delta t) = \exp(-iH\delta t) \approx \exp(-iV\delta t/2) \times \exp\left(-i\sqrt{(-i\nabla + \mathbf{A})^2c^2 + m_0^2c^4}\delta t\right) \times \exp(-iV\delta t/2) + O(\delta t^3). \quad (32)$$

The propagator $\exp(-iV\delta t/2)$ is diagonal in the real-space representation and easy to calculate. For the other propagator $\exp[-i\sqrt{(-i\nabla + \mathbf{A})^2c^2 + m_0^2c^4}\delta t]$, it will be dealt with using the Krylov-subspace method. The error caused by the splitting operator method is much less than that in Refs. [10,11]. Because the magnitude for the commutator of two parts is much smaller than m_0c^2 here, whose leading order is $\nabla^2V(\mathbf{r}, t) - i\nabla V \cdot \mathbf{A}(\mathbf{r}, t)$. Here we shall demonstrate how the propagator $\exp[-i\sqrt{(-i\nabla + \mathbf{A})^2c^2 + m_0^2c^4}\delta t]\psi$ is evaluated using a modified Krylov-subspace method. In the standard method, the Krylov subspace is spanned by $\{\psi, \hat{H}\psi, \hat{H}^2\psi, \dots, \hat{H}^{N-1}\psi\}$ (16), where $\hat{H} = \sqrt{(-i\nabla + \mathbf{A})^2c^2 + m_0^2c^4}$ here. Expanding the square-root operator in \hat{H} in the Taylor series of $\hat{T} = (-i\nabla + \mathbf{A})^2$, we will get the subspace also can be spanned by vectors $\hat{T}^n\psi$. We redefine a Krylov subspace as $K_N = \{\psi, \hat{T}\psi, \hat{T}^2\psi, \dots, \hat{T}^{N-1}\psi\}$. The Hermitian operator \hat{T} is easily represented as a tridiagonal matrix T_K in this redefined Krylov subspace using the standard Lanczos method. Then the operator $\sqrt{(-i\nabla + \mathbf{A})^2c^2 + m_0^2c^4}$ also can be expressed in the subspace as the method used in the real space [51]

$$Z^{-1}T_KZ = E, \quad \sqrt{T_Kc^2 + m_0^2c^4}\mathbf{I} = Z\sqrt{Ec^2 + m_0^2c^4}Z^{-1}. \quad (33)$$

Since the Krylov subspace usually has the order of $20 \sim 40$, the demanded computing requirement for diagonalizing the matrix T_K in this subspace is substantially lower than that in the full real space. As a result, the evolution of the wave function can be written as

$$\psi(t + \delta t) = (q_0 \quad q_1 \quad \dots \quad q_{N-1})Ze^{-i\sqrt{Ec^2 + m_0^2c^4}\delta t}Z^\dagger \begin{pmatrix} 1 \\ 0 \\ \vdots \\ 0 \end{pmatrix}. \quad (34)$$

The nonlocality of the square-root operator now is reflected in the fact that the operator is expressed as a dense matrix in the subspace K_N , rather than in the real space. Additionally, the matrix T_K is a positive-definite matrix. This precludes the existence of solutions with negative kinetic energies, which will arise in the SSE. A sketch for our scheme is plotted against the classical schemes in Fig. 1. The whole wave-function space is expanded in different orders of the Krylov subspace and the relativistic correction. Generally speaking, the importance of the component decreases with the order of both relativistic correction and Krylov subspace. In the sketch, we note that a component like $\hat{T}^n\psi$ may come from several sources, which are contributed from different relativistic correction orders and different Krylov subspace orders. Since we exactly solve the square-root operator in the subspace K_N ,

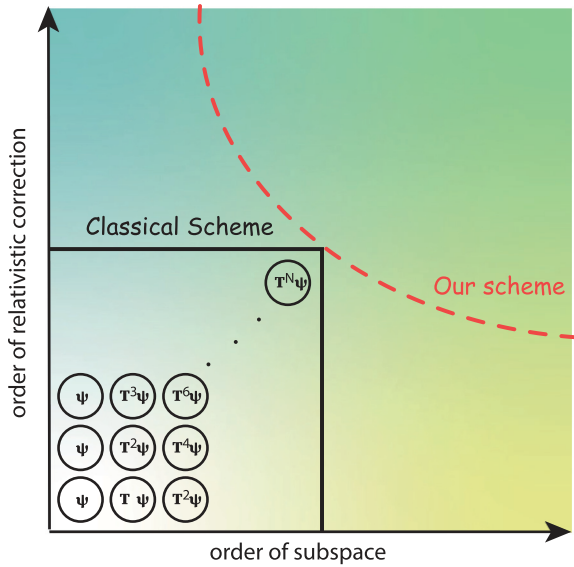


FIG. 1. The sketch depicts our scheme for the propagator of the $\sqrt{(-i\nabla + \mathbf{A})^2 c^2 + m_0^2 c^4}$ against the classical scheme. The horizontal coordinate represents the order of the subspace and the vertical coordinate represents the order of the relativistic correction. Each black circle represents a component for the corresponding order of subspace and relativistic correction. The red dashed line represents our scheme, whereas the black solid line represents the classical Arnoldi scheme.

all the components lower than $\hat{T}^N \psi$, which are represented by the area enclosed by the red dashed line and axes, are covered by our scheme. Whereas, the classical scheme only covers the area enclosed by the black solid line and axes. For the same amount of matrix-vector multiplications, it is obvious that our scheme covers more area.

Due to restricted problems induced by the boundary condition at $r = 0$, the propagation method cannot perform at its best in the cases we study. However, the method itself is still instructive for studying the dynamics of the equation with the nonlocal operator. It provides an available approach to deal with the time-dependent propagation problem with the nonlocal operator approximately.

IV. NUMERICAL RESULTS

In this section, we first calculate some eigenvalues and eigenstates for different equations in the field-free condition. The results from different grid discretization schemes are also compared. Then the photoionization in the perturbative regime and the relativistic regime are investigated. The

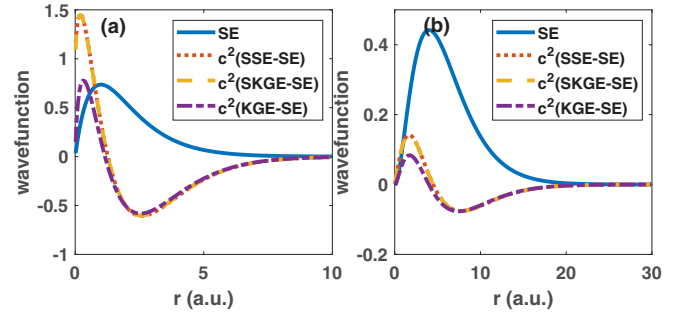


FIG. 2. The eigenstates' radial wave function for the SE (blue solid line), and the correction for the SSE (red dotted line), the SKGE (yellow dashed line), and the KGE (purple dashed-dotted line). The results of $1s$ and $2p$ states are shown in (a) and (b), respectively. All the corrections have been multiplied by c^2 .

relativistic and nondipole effects are discussed. After that, we concentrate on the relativistic effects in the HHG. The agreement of the results from the KGE and the SKGE within the first-order relativistic correction is checked in both photoionization and HHG. In the following, we shed some light on the charge conservation and the particle pair production in the KGE. Finally, the parallel efficiency of programs is demonstrated.

A. Eigenvalues and eigenstates

In order to evaluate the validity of the Hamiltonian and the convergence of the grids, the simplest method is to solve the eigenvalues and the eigenvectors of the Hamiltonian matrix represented on the corresponding basis. Taking the Coulomb potential with unit charge (the hydrogen atom) as an example, we calculate the first few eigenvalues of SE, SSE, KGE, and SKGE with different finite-element numbers N_{FE} and various basis numbers N_B in each finite element. In addition, the Gauss-Lobatto quadrature and the Gauss-Radau quadrature are employed in the first finite element to solve the $1s$ state individually for comparison. Of course, the Gauss-Lobatto quadrature is employed in the other elements in both cases. The exact eigenvalues of the SE and KGE are listed in the following as a reference. The eigenvalues of the $1s$ state for the SE and the KGE are $E = -0.5$ and $E = -0.500033285819$, respectively. The $2p$ state has an eigenvalue of $E = -0.125$ for the SE and $E = -0.125000970740$ for the KGE. Provided that the grid is uniform and $r_{\max} = 100$, the eigenvalues of $1s$ calculated for different equations are listed in Tables I and II, while Table III is for $2p$ states. These numerical results allow us to draw some preliminary conclusions. First, the SE's eigenvalues converge to the precise value more quickly compared to other equations. This is due to the fact that for such a nonrelativistic equation, the high-energy component is not

TABLE I. Eigenvalues of $1s$ state using the Gauss-Lobatto quadrature in the first element.

Grid	SE	SSE	SKGE	KGE
$N_{FE} = 28$ $N_B = 8$	-0.499999783224	-0.500026280974	-0.500026271369	-0.500026274050
$N_{FE} = 56$ $N_B = 8$	-0.499999999956	-0.500029904169	-0.500029879830	-0.500029888175
$N_{FE} = 56$ $N_B = 10$	-0.500000000000	-0.500031197852	-0.500031155683	-0.500031171425
$N_{FE} = 112$ $N_B = 8$	-0.500000000000	-0.500031619821	-0.500031565544	-0.500031586991

TABLE II. Eigenvalues of $1s$ state using the Gauss-Radau quadrature in the first element.

Grid	SE	SSE	SKGE	KGE
$N_{FE} = 28$ $N_B = 8$	-0.500001466548	-0.500034779067	-0.500034746329	-0.500034757279
$N_{FE} = 56$ $N_B = 8$	-0.500000000591	-0.500033329593	-0.500033257986	-0.500033286058
$N_{FE} = 56$ $N_B = 10$	-0.500000000001	-0.500033356448	-0.500033234294	-0.500033285800
$N_{FE} = 112$ $N_B = 8$	-0.499999999999	-0.500033371049	-0.500033234293	-0.500033285974

as significant as others. So the eigenvalues can converge with relatively sparse grids. Second, the eigenvalues of the SSE are consistently lower than those of SKGE and KGE because the SSE lacks positive higher-order corrections. Additionally, the KGE's eigenvalues are lower than those of SKGE, which supports our earlier claim that the SKGE is more stable. Third, the eigenvalues of the $2p$ state converge more quickly than those of $1s$ state. This is because the high-energy part is less important for the $2p$ state. In other words, the boundary condition is smoother for the $2p$ state. Fourth, the SE's eigenvalues converge slower to the exact value in the Gauss-Radau quadrature compared with the Gauss-Lobatto quadrature. It may be attributable to the fact that the fixed boundary condition of the SE $\chi(0) = 0$ is used in the Gauss-Lobatto quadrature. However, other relativistic equations' eigenvalues converge faster in the Gauss-Radau quadrature because the operator p^4 and higher-order derivatives in the Gauss-Radau quadrature are more accurate, which has been explained in Sec. III B.

From the above observations, it appears that we should use the Gauss-Radau quadrature rather than the Gauss-Lobatto quadrature in the first finite element for a relativistic problem. But, the Gauss-Radau quadrature has a disadvantage: there exist approximations in its matrix expression of the first derivative operator, which is demonstrated in Appendix A. In the Hamiltonian, the first derivative operator is present in the dipole interaction operator, while the fourth and higher-order derivatives only appear in the relativistic correction operator. Considering the relativistic correction is much smaller than the nonrelativistic dipole interaction in most conditions, we use the Gauss-Lobatto quadrature in the first finite element in the following. And it should be noted that the problems of the Gauss-Lobatto quadrature only are induced by the boundary conditions. The Gauss-Lobatto quadrature itself performs quite well in other cases when the boundary conditions are smooth enough.

Now let us discuss the eigenstates of different equations. The eigenstate of the KGE here is referred to $\psi = \Psi_1 + \Psi_2$, in which Ψ_1 and Ψ_2 are components in Eq. (4). Since the relativistic corrections of the wave function are insignificant for the hydrogen atom, the eigenstates' differences between the SE and the other equations are multiplied by c^2 to be

compared with the original SE's eigenstate. For the configuration of $r_{\max} = 30$ a.u., $N_{FE} = 112$ and $N_B = 8$, the radial wave function χ of the $1s$ and $2p$ states is displayed in Fig. 2. First, it is obvious that the relativistic correction is larger in the $1s$ state because the $1s$ state has more high-energy components. In addition, it demonstrates that the eigenstates of the SKGE are almost identical to those of SSE on the order of $1/c^2$. This coincides with what we are expecting, i.e., they remain the same until the $1/c^2$ order. But, there exist unphysical eigenstates for SSE when the grid density increases. This phenomenon is illustrated in Fig. 3. The number of bases is fixed at $N_B = 10$ and $r_{\max} = 30$ a.u. in this case. Whereas, the number of finite elements is changed from $N_{FE} = 142$ (a) to $N_{FE} = 143$ (b). The eigenstates are normal when $N_{FE} = 142$. However, substantial unphysical oscillations emerge in eigenstates when $N_{FE} = 143$. The oscillatory shape depends on the grid configuration. This behavior is very similar to the spurious states in the numerical solutions to the Dirac equations [9,57,58]. These unphysical situations can be avoided in the SKGE.

It is also worth mentioning that the eigenstates of KGE and SKGE in Fig. 2 differ in the order of $1/c^2$. This argument has been made in Sec. III A as well. The approximate relationship between them is given in Eq. (27). We have checked it numerically. Furthermore, the bound states of the KGE can also be given analytically. Taking the $1s$ state of the hydrogen atom as an example, its eigenstate is $\psi(r) = \mathcal{N}r^{1/2-\sqrt{1/4-1/c^2}} \exp(-cr\sqrt{1/2-\sqrt{1/4-1/c^2}})$ [59], where \mathcal{N} is a normalized constant. It agrees, at least in the $O(1/c^2)$ order, with our numerical results. This demonstrates the accuracy of our Hamiltonians and numerical methods.

B. Laser-induced ionization

In this subsection, the programs will be applied to an important topic in the strong-field physics, which is the laser-induced ionization. It has been studied quite thoroughly in the nonrelativistic conditions. Many interesting phenomena including the suppression of the low-energy peaks, the Freeman resonance, and the high-energy plateau structure have been observed in the experiments and explained in the theory. The

TABLE III. Eigenvalues of $2p$ state using the Gauss-Lobatto quadrature in the first element.

Grid	SE	SSE	SKGE	KGE
$N_{FE} = 28$ $N_B = 8$	-0.124999999892	-0.125000970674	-0.125000970612	-0.125000970613
$N_{FE} = 56$ $N_B = 8$	-0.125000000000	-0.125000970782	-0.125000970712	-0.125000970802
$N_{FE} = 56$ $N_B = 10$	-0.125000000000	-0.125000970783	-0.125000970711	-0.125000970580
$N_{FE} = 112$ $N_B = 8$	-0.125000000000	-0.125000970783	-0.125000970717	-0.125000970795

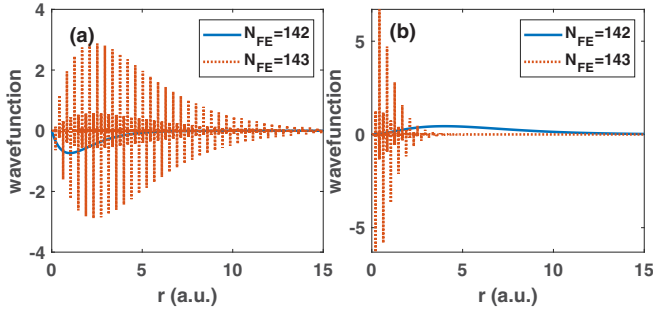


FIG. 3. The eigenstate radial wave function for the SSE in the configuration of $N_{\text{FE}} = 142$ (blue solid line) and of $N_{\text{FE}} = 143$ (red dotted line). The results of the $1s$ and $2p$ states are shown in (a) and (b), respectively.

relativistic effects are not important in most conditions for the ionization problem, but they also can induce measurable variations of the results in some extreme parameters. These effects may result from many aspects of relativistic corrections, such as initial state corrections, scattering state corrections, and light-matter interaction corrections. Their significances vary, depending on the laser pulse parameters and photoelectron energy ranges. Some previous studies have used approximation methods to discuss the relativistic ionization in theory [60–62]. However, it is commonly acknowledged that the TDSE is one of the most effective theories to study the ionization problem. In this work, we extend the TDSE to the time-dependent SKGE and the time-dependent KGE to study the relativistic effects accurately. Some researchers have used the time-dependent relativistic equations to study the relativistic ionization by the infrared laser pulse [8,63] and the other focused on the relativistic ionization by the extreme ultraviolet (XUV) pulse [4,16]. We mainly concentrate on the latter in this subsection.

Let us start from the very basic case, i.e., the one-photon ionization in the weak field. The $1s$ state of the hydrogen atom is irradiated by a linearly polarized laser pulse with a carrier frequency $\omega = 2$ a.u. and a peak intensity $I = 1 \times 10^{13}$ W/cm². The full width at half-maximum (FWHM) of the Gaussian pulse is $\tau = 2 \times 2\pi/\omega$. The expression of the vector potential can be written as

$$\mathbf{A}(\mathbf{r}, t) = -\frac{\sqrt{I_0}}{\omega} \exp\left(-\frac{4 \ln 2 t^2}{\tau^2}\right) \sin(\mathbf{k} \cdot \mathbf{r} - \omega t) \hat{\mathbf{e}}_z. \quad (35)$$

For the sake of simplicity, the dipole approximation is used in the calculation, which means the space dependence of the laser is ignored. The radial coordinate ranges from 0 to $r_{\text{max}} = 300$ a.u., and it is split into 168 finite elements, with 10 basis functions in each element. The maximum angular quantum number is set to 5. As for the propagation parameters, the time step is set to $dt = 0.001$ a.u. and the order of the Krylov subspace is set to 40. Naturally, all the configurations are kept being identical for different equations to ensure that no nonphysical influences have an impact on the result. There is no absorbing scheme in our calculations. The contributions from the reflection of the boundary are very small and can be eliminated when we make the differences for different equations.

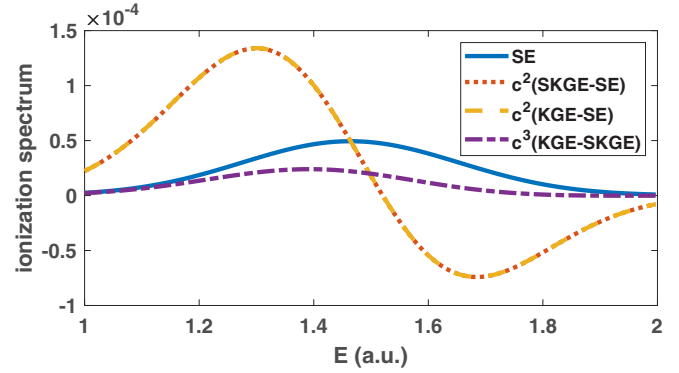


FIG. 4. The energy differential ionization spectrum for the SE is shown in the blue solid line. While the difference between SKGE and SE is shown in the red dotted line and the difference between KGE and SE is shown in the yellow dashed line, both of which have been multiplied the factor c^2 . The red dotted line and the yellow dashed line are nearly overlapping. The purple dashed-dotted line represents the difference between the KGE and the SKGE multiplied the factor c^3 .

In the perturbative regime such as the laser parameters mentioned above, the main relativistic effect comes from the correction of the initial state. As shown in Table I, the relativistic correction makes the eigenvalues of the initial state lower, so the corresponding one-photon ionization peak also locates at lower energy. The ionization spectra of different equations and their differences have been shown in Fig. 4. To make the differences visible, we multiply a factor c^2 or c^3 by them. First, it is easy to find that the relativistic effects make the ionization spectrum have more components at the low-energy regime and fewer components at the high-energy regime. This confirms our hypothesis that the peak would shift to the left. And the results of the KGE and the SKGE are highly consistent at $O(1/c^2)$, which also confirms our analytical conclusion. Then, if one wants to see the difference between KGE and SKGE, a larger factor c^3 needs to be multiplied. The results show that the ionization probability is larger in the KGE, particularly for the low-energy part.

The relativistic corrections of the interaction and the final state may become significant as the laser's intensity and frequency increase. An example in Ref. [16] will be reproduced in the following. The laser parameters are $\omega = 50$ a.u., $E = 60$ a.u., and $\tau = 4$ cycles in this case. To ensure the convergence of the high-energy states, smaller time steps and denser spatial grids are employed. The maximum radial range does not change ($r_{\text{max}} = 300$ a.u.), but it is split into 784 finite elements now, each of which has 10 basis functions. The maximum angular quantum number is set to 10. Regarding the propagation parameters, the time step is set to $dt = 0.0001$ a.u. and the order of the Krylov subspace is still 40. Although the program can run stably with much bigger time steps, but such a small time step is needed when we want to obtain fully convergent results for examining the difference between KGE and SKGE.

The authors also discussed the nondipole effect in Ref. [16]. So, we accordingly calculate a SE case that takes the first-order nondipole effect into account. The vector potential

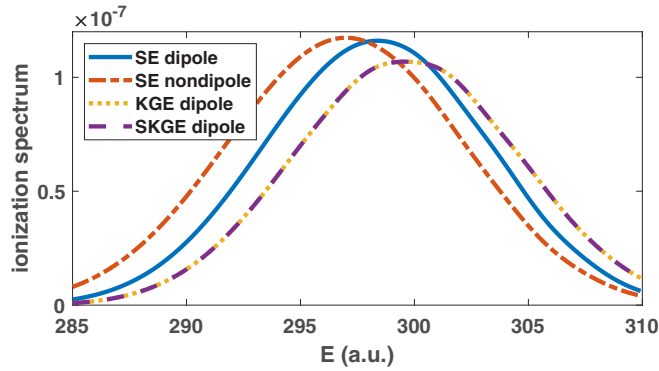


FIG. 5. The energy differential ionization spectrum for the SE within the dipole approximation is shown in the blue solid line. The corresponding SE's result beyond the dipole approximation is shown in the red dashed-dotted line. Two relativistic results within the dipole approximation are represented in the yellow dashed line and purple dotted line, respectively, which are nearly identical.

of the laser pulse is expanded to the first order around a point \mathbf{r}_0 ,

$$A(\mathbf{r}, t) \approx A(\mathbf{r}_0, t) + \frac{\hat{\mathbf{k}} \cdot (\mathbf{r} - \mathbf{r}_0)}{c} E(\mathbf{r}_0, t), \quad (36)$$

where $E(\mathbf{r}_0, t)$ is the electric field at \mathbf{r}_0 and $\hat{\mathbf{k}}$ is the propagation direction of the laser. The Hamiltonians related to the leading-order nondipole effect are in the order of $1/c$, which will induce an average momentum shift in the order of $1/c$ along the propagation direction. As a result, the effect reflected in the energy differential spectrum is in the order of $1/c^2$, which is comparable with the leading-order relativistic corrections. The six-photon peak calculated from different equations is shown in Fig. 5. The results from two relativistic equations are still very similar. We can get the same conclusion as that in Ref. [16], which is the nondipole effect induces a redshift of the multiphoton peaks and the relativistic effect induces a blueshift.

C. High harmonic generation

The HHG is another important topic in strong-field physics. The phenomenon can be understood in a classical way: After absorbing an integer number of photons, the electron is ionized and then recollides with the nucleus to recombine with the ground state by releasing a high-energy photon. For a simple atomic system with the spherical symmetry, the even harmonics will vanish due to the interference. One can only observe the odd harmonics. A well-known feature of the HHG is the plateau structure, which has been successfully interpreted by the semiclassical three-step model [64]. The HHG is present in numerous systems with different laser pulses, despite the fact that it is detected and explained for the atoms in the moderate-intensity infrared laser at first. To observe the relativistic effect of the HHG, highly charged ions and high-intensity lasers are needed. Some previous studies used the strong-field approximation (SFA) to calculate the HHG in such extreme conditions [65–67]. The relativistic results are compared with the nonrelativistic results. And others used the two-dimensional time-dependent SSE and the

soft-core Coulomb potential to calculate the HHG including the relativistic corrections [14,68]. In this subsection, the relativistic HHG results from the time-dependent SKGE and KGE are contrasted with the nonrelativistic HHG results from the TDSE. We have confirmed the nondipole correction is much smaller than the relativistic correction in this situation. So, the dipole approximation is applied for the results shown here. Additionally, the acceleration gauge is used to calculate the HHG along the laser pulse propagation direction [69]. If the laser polarization direction is along the z axis, for the SE and the SKGE, the yield of the HHG can be written as

$$\text{HHG}(\Omega) = \int_{-\infty}^{\infty} dt e^{-i\Omega t} F(t) \langle \psi(t) | \frac{\partial}{\partial z} V(r) | \psi(t) \rangle, \quad (37)$$

where $F(t)$ is a Gaussian window function. With respect to the KGE, the pseudometric η should be inserted in the inner product

$$\text{HHG}(\Omega) = \int_{-\infty}^{\infty} dt e^{-i\Omega t} F(t) \langle \Psi(t) | \eta \frac{\partial}{\partial z} V(r) | \Psi(t) \rangle. \quad (38)$$

We consider the case that a Ne^{9+} ion is irradiated by a linearly polarized laser pulse with a carrier frequency $\omega = 8$ a.u. and a peak intensity $I = 1 \times 10^{20}$ W/cm². The FWHM of the Gaussian laser pulse is $\tau = 5$ cycles. The order of cutoff HHG is not large in this case, so the maximum angular quantum number is set to 20. The maximum radial coordinate is $r_{\text{max}} = 100$ a.u., the radial space is split into 448 finite elements uniformly, each of which has 10 basis functions. The propagation parameters are identical to those of Fig. 5. From Fig. 6(a) with the logarithmic scale, we can observe odd HHG peaks and a clear plateau structure for all the results, which are comparable to the HHG by infrared lasers with moderate intensities. In Figs. 6(b) and 6(c) with the linear scale, the relativistic effect can be shown more clearly, which enhances HHG production in the plateau regime and decreases the HHG production in the cutoff regime.

D. Charge conservation and particle pair production

During the process of the time-dependent propagation, the total charge should be conserved for all the equations in principle. Specifically, the norm of the wave function that represents the charge should be unchanged in the SE and the SKGE because Hamiltonians are Hermitian and propagators are unitary. However, the Hamiltonian is pseudo-Hermitian in the KGE, so the charge is still conserved but the wavefunction norm is not. In the actual calculation, the charge conservation may be violated due to the numerical errors that come from a variety of aspects. So, it is a good way to assess the accuracy of the program by checking the charge conservation. Take the second case in Sec. IV B as an example, the evolutions of the charge deviation for the three programs are plotted in Fig. 7(a). It is obvious that all the changes of the charge are controlled in a very tiny range, which is smaller than the relativistic correction of the first few orders. Therefore, there is no cause to worry about the relativistic correction's inaccuracy brought by the numerical error that accumulated in the propagation. Nevertheless, we can still improve the accuracy of the charge conservation. The loss of the orthogonality of vectors during the Gram-Schmidt process

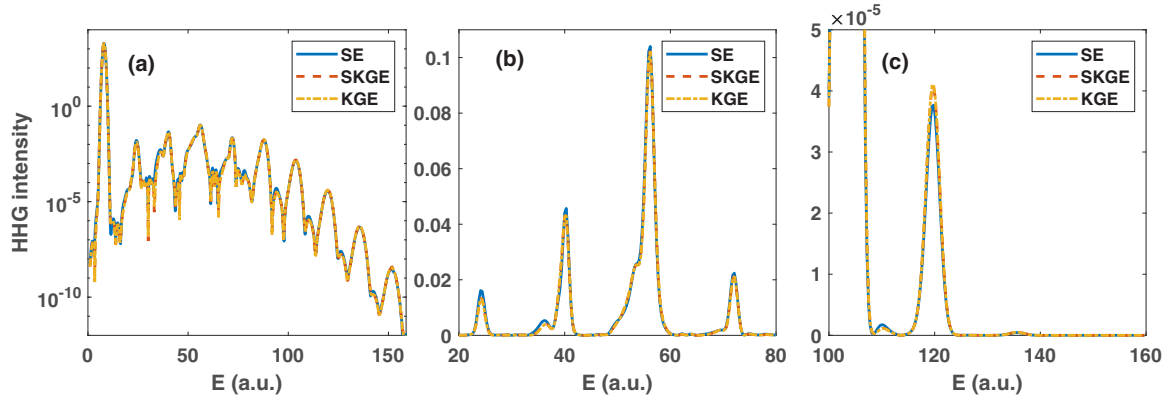


FIG. 6. The HHG spectrum for the SE in the dipole approximation is shown in the blue solid line. Two relativistic results within the dipole approximation are shown in the red dashed line and yellow dash-dotted line, respectively. The results are plotted in the logarithmic coordinates (a), linear coordinates for the low-energy regime (b) and the high-energy regime (c).

is a severe problem existing in the Arnoldi or the Lanczos method. It contributes a significant proportion of errors. A simple way to solve the problem is the reorthogonalization [70]. The corresponding results with the reorthogonalization are shown in Fig. 7(b). We can see that the error has been significantly decreased, especially for the SKGE and the KGE.

Now, let us focus solely on the KGE. An important point that makes it different from the other two equations is that it has solutions with negative energy. This indicates the equation allows for particle pair production process, in which a pair of particle and antiparticle is created together. It does not break the charge conservation we discussed above. This process can occur with the assistance of the external electromagnetic field [71–74] or ion collisions [75]. We mainly concentrate on the former in this paper. For a one-particle relativistic equation, the process can be regarded as the transition from a negative-energy state to a positive-energy state [76,77]. It also can be understood by tunneling or multiphoton pictures, which is similar to the ionization process [77]. The pair production can happen for both fermions and bosons when the field becomes extremely strong (close to the Schwinger field $E = 1.3 \times 10^{16}$ V/cm) or the photon energy is extraordinarily high. It should be noted that the single plane-wave laser field can not create pairs from the vacuum

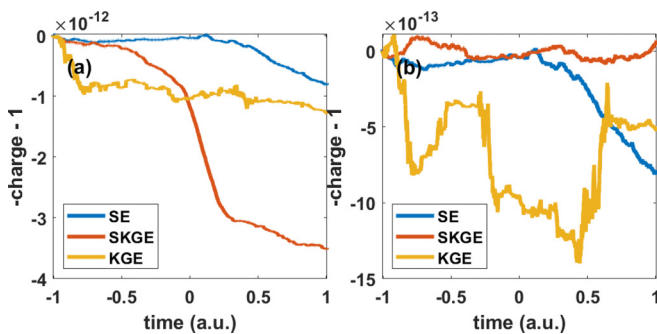


FIG. 7. The time-dependent charge evolution for the SE is shown in the blue line. The red line represents the SKGE result, whereas the yellow line represents the KGE result. All the charges have been subtracted by 1 to show the deviation. The results without and with the reorthogonalization are shown in (a) and (b), respectively.

[77]. This process can be possible with the assistance of another identical counterpropagating laser pulse [12,77] or the Coulomb potential [78–81]. The nondipole effect is very important in some conditions [12], but it is ignored for the purpose of simplifying the calculation in our study. The laser field is represented as an oscillating electric field in time as Ref. [77]. The grid configuration is as follows: the maximum range of the coordinate is $r_{\max} = 5$ a.u., and it is split into 448 finite elements, each of which has 10 basis functions. The corresponding eigenvalues without any potential are shown in Fig. 8(a). There are two symmetry branches with an energy gap of $2m_0c^2$. The maximum angular quantum number is set to 5. And the propagation parameters used here are also identical to those of Fig. 5. As for the parameters of the laser pulse, the FWHM is $\tau = 5$ cycles and intensities and frequencies are shown in Fig. 8(b). We show two consequences of cases varying with the intensities in this figure: one corresponds to the one-photon absorption and the other corresponds to the two-photon absorption. The initial states are set to be the highest state on the negative-energy branch in both cases. We can find that the production probabilities varied with the laser

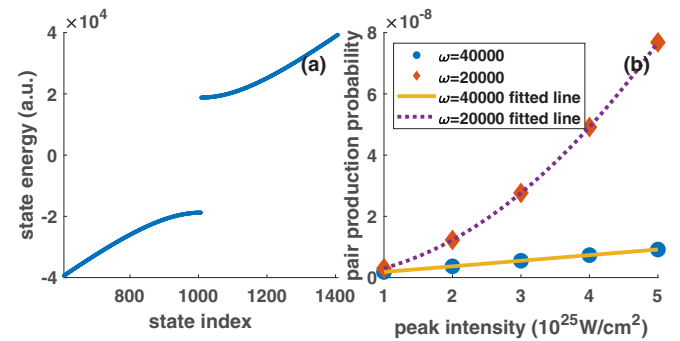


FIG. 8. (a) The eigenvalues of KGE are displayed with the indices in the blue solid line. (b) The pair creation probabilities obtained from the KGE change with the laser intensities for two different frequencies. The result of $\omega = 40\,000$ and $20\,000$ a.u. is shown in the blue circle and the red diamond, respectively. The corresponding linear and quadratic fitted lines are plotted in the yellow solid line and the purple dotted line.

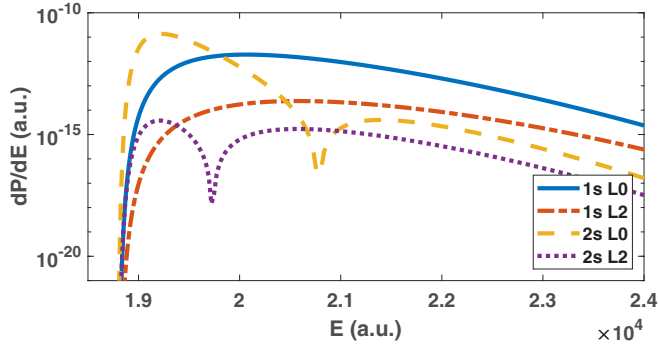


FIG. 9. The energy differential pair creation probabilities obtained from the KGE for different bound states and different angular quantum numbers of free states are shown against the energy of the free particle. The blue solid line represents the condition of the $1s$ state and $\ell = 0$ for the free state. The red dashed-dotted line represents the condition of the $1s$ state and $\ell = 2$ for the free state. The yellow dashed line represents the condition of the $2s$ state and $\ell = 0$ for the free state. The purple dotted line represents the condition of the $2s$ state and $\ell = 2$ for the free state.

intensity fit with the corresponding scaling law very well. This demonstrates the reliability of the program on the pair production.

If there exists a Coulomb potential, the created particles may be in bound states. In contrast to the free-free pair creation process, this is the so-called bound-free pair creation process, which is generally considered more difficult to happen. It has some different behaviors [79,81] from the free-free process. A bound-free pair creation process can be regarded as the transition from a negative free state to a positive bound state (there are no negative bound states in most conditions). When the transition probability is very low, its value is equivalent to that of the corresponding reversed process. So, we set the initial state to the positive bound state and observe the population of various negative-energy states after the laser pulse. In Fig. 9, we adjust laser intensity to 1×10^{25} W/cm², laser frequency to $\omega = 20\,000$ a.u., and the nuclear charge to $Z = 10$, then calculate the energy differential production probabilities for different bound states and different angular quantum numbers of negative-energy states.

E. Computational performance

To show the efficiency and the parallel performance of different programs, we execute programs for the same computation task on different numbers of cores. Here the case in Sec. IV C is taken as the example. And the model of the central processing unit (CPU) that we used is Intel Xeon E5-2620@2.10GHz. The test results are represented in Fig. 10. For the ideal condition, the wall time should be inversely proportional to the number of cores for a given task, which means the relation between the wall time and cores is a straight line in the logarithmic-logarithmic coordinate. It is actually the case the fitted straight lines indeed can match the actual time cost very well. This illustrates the high parallel performance of our programs. In addition, we can find that the wall times of SKGE and SE are quite close, while the KGE costs four times. It indicates the program's time consumption is dominated

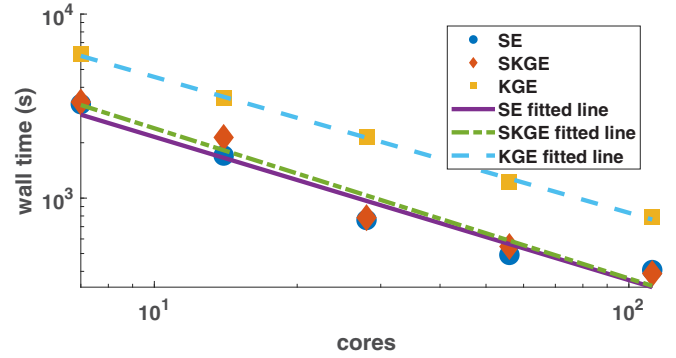


FIG. 10. The wall times are shown against different cores for different programs for the same computation task. The results of SE are shown in blue circles and the corresponding fitted line is the purple solid line. The results of SKGE are shown in red diamonds and the corresponding fitted line is the green dashed-dotted line. The results of KGE are shown in yellow squares and the corresponding fitted line is the blue dashed line.

by the matrix-vector multiplication because the number of Hamiltonian matrix elements is the same for the SKGE and SE, and four times more for KGE. If no negative-energy states are needed, the SKGE and the SSE are better choices to study the first-order relativistic corrections for the sake of efficiency.

V. CONCLUSIONS AND OUTLOOK

We have solved the SKGE and KGE with time-dependent electromagnetic fields in the three-dimensional real space using Krylov-subspace methods. The non-Hermitian Arnoldi method is successfully applied in the propagation of the KGE. Whereas, the propagator of the square-root operator in the SKGE is expressed in a redefined Krylov subspace. The programs can deal with various cases of the light-matter interaction, from the linear regime to the nonlinear regime. We test the programs in a series of cases about the photoionization, HHG, and the particle pair production process. The results are compared with those from the usual TDSE, which verifies a conclusion that we can prove analytically: These two equations are identical for all the observables up to and only up to the first relativistic corrections. Additionally, the computational performances of different equations are also contrasted. The results show that SKGE consumes fewer computational resources than KGE. If the negative-energy levels are not crucial to the physical process (a counterexample is pair production), the SKGE is a good alternative to the KGE in the relativistic perturbative domain.

Finally, we demonstrate that the programs perform quite well when parallelized. They are thus easily adaptable to more complex or more extreme scenarios, which will facilitate real-time and real-space investigations on relativistic quantum dynamics.

ACKNOWLEDGMENTS

This work is supported by the National Natural Science Foundation of China (NSFC) under Grants No. 12234002, No.

92250303, and No. 11961131008, and by the National Key R&D Program of China under Grant No. 2018YFA0306302.

APPENDIX A: SCHEME OF GRID DISCRETIZATION FOR REAL SPACE

The scheme of grid discretization for the real space will be shown in this Appendix. First, let us take the wave function $\psi(\mathbf{r})$ of the SE as an example. It can be expanded in terms of spherical harmonics $Y_{\ell m}(\hat{\mathbf{r}})$ in the azimuthal coordinate

$$\begin{aligned}\psi(\mathbf{r}) &= \sum_{\ell=0}^{\ell_{\max}} \sum_{m=-\ell}^{m=\ell} R_{\ell m}(r) Y_{\ell m}(\hat{\mathbf{r}}) \\ &= \frac{1}{r} \sum_{\ell=0}^{\ell_{\max}} \sum_{m=-\ell}^{m=\ell} \chi_{\ell m}(r) Y_{\ell m}(\hat{\mathbf{r}}),\end{aligned}\quad (\text{A1})$$

where $\hat{\mathbf{r}} = \mathbf{r}/r$, ℓ is the angular quantum number and m is the magnetic quantum number. In this way, the inner product of the wave function in the three-dimensional space can be reduced into the radial integral and the sum for various $\{\ell, m\}$ indices

$$\langle \psi_1(\mathbf{r}) | \psi_2(\mathbf{r}) \rangle = \sum_{\ell=0}^{\ell_{\max}} \sum_{m=-\ell}^{m=\ell} \int_0^{r_{\max}} \chi_{1\ell m}^*(r) \chi_{2\ell m}(r) dr. \quad (\text{A2})$$

If one wants to calculate the integral numerically in an efficient way, the Gaussian quadrature is a good choice. Taking a function defined in $[-1, 1]$ as an example, its integral can be written as the sum at n different points x_j with different weights w_j :

$$\int_{-1}^1 f(x) dx \approx \sum_{j=1}^n w_j f(x_j). \quad (\text{A3})$$

The integral is exact for polynomials of degree $2n - 1$ or less, which depends on the location of points. The Gauss-Legendre, Gauss-Radau, and Gauss-Lobatto quadratures are the three most prevalent quadratures if no weight function is provided [82]. In the Gauss-Legendre quadrature, the points x_j contain neither the left end point nor the right end point, the integral is exact for polynomials of degrees up to $2n - 1$. And either the left end point or the right end point is contained in the Gauss-Radau quadrature, it is exact for polynomials of degrees up to $2n - 2$. Whereas both the left and the right end points are contained in the Gauss-Lobatto quadrature, it is exact for polynomials of degrees up to $2n - 3$. By these methods, we only need to calculate and record the value of the integrand on a few points in the program, which saves a lot of the memory and computation. In our calculation, we want to express the wave function $\chi(r)$ using some local functions. Thus, the FE-DVR is employed to discretize the radial coordinate r . The entire radial space, ranging from 0 to r_{\max} , is partitioned into a number of finite elements. The integral can be calculated using the Gaussian quadrature in each finite element $[r_i, r_{i+1}]$ with a scaling factor

$$\int_{r_i}^{r_{i+1}} f(r) dr \approx \sum_{j=1}^n w_{i,j} f(r_{i,j}), \quad (\text{A4})$$

where $w_{i,j} = w_j(r_{i+1} - r_i)/2$ and $r_{i,j} = [(r_{i+1} + r_i) + x_j(r_{i+1} - r_i)]/2$. In order to connect different finite elements, we need to know the value of the junction of different elements. As a result, the Gauss-Lobatto quadrature is used in the elements that do not locate outermost, the corresponding points x_j satisfy the relation

$$\frac{(x_j^2 - 1)P'_{n-1}(x_j)}{n-1} = x_j P_{n-1}(x_j) - P_{n-2}(x_j) = 0, \quad (\text{A5})$$

where $P_n(x)$ is the Legendre polynomial of degree n defined at $x \in [-1, 1]$ and P'_n is its derivative. The corresponding weights are given by

$$w_j = \frac{2}{n(n-1)P_{n-1}^2(x_j)}. \quad (\text{A6})$$

For the outermost finite element, one can still employ the Gauss-Lobatto quadrature, or use the Gauss-Radau quadrature instead. In the Gauss-Radau quadrature, the series x_j locate at the points that satisfy

$$P_n(x) - P_{n-1}(x) = 0. \quad (\text{A7})$$

The corresponding weights are given by

$$w_j = \frac{1 + x_j}{[nP_{n-1}(x_j)]^2}. \quad (\text{A8})$$

For both quadratures, Lagrange interpolation polynomials of order n can be constructed in a finite element on the basis of $r_{i,j}$:

$$L_{i,j}(r) = \begin{cases} \prod_{k \neq j} \frac{r - r_{i,k}}{r_{i,j} - r_{i,k}}, & r \in [r_i, r_{i+1}] \\ 0, & r \notin [r_i, r_{i+1}]. \end{cases} \quad (\text{A9})$$

They are the basis functions of the wave function. It is obvious that each polynomial is only nonzero on one point among all the points $r_{i,j}$:

$$L_{i,j}(r_{i,j'}) = \delta_{i,i'} \delta_{j,j'}. \quad (\text{A10})$$

This good property enables the value on a point $r_{i,j}$ is only associated to one basis function. For the Gauss-Lobatto quadrature, the inner product of two interpolation polynomials in the same finite element is an integral of a polynomial of degree $2n - 2$, which can be determined using Eq. (A4), approximately,

$$\begin{aligned} & \int_{r_i}^{r_{i+1}} L_{i,j}(r) L_{i,k}(r) dr \\ & \approx \sum_{m=1}^{m=N} L_{i,j}(r_{i,m}) L_{i,k}(r_{i,m}) w_{i,m} = \delta_{j,k} w_{i,j}. \end{aligned} \quad (\text{A11})$$

The accuracy of the Gauss-Lobatto quadrature is only lower than the integrand by one order. As a result, only $2n - 2$ order strongly oscillating polynomials in the integrand are inaccurate. These elements are typically absent from physical states. So it is believed the inner product of wave function on this basis is quite accurate numerically, not to mention that Eq. (A11) is strictly correct in Gauss-Radau quadratures. If the new basis functions are defined as $f_{i,j}(r) = L_{i,j}(r)/\sqrt{w_{i,j}}$, they form a group of normalized orthogonal bases in this

element. After introducing the configuration in one finite element, the method for connecting different elements will be demonstrated. We use the method called the bridge function method here. A bridge function is created by combining the first basis of the later element and the last basis of the former element. The basis on the boundary of element is specified as $f_{\text{bridge}}(r) = [L_{i,n}(r) + L_{i+1,1}(r)]/\sqrt{w_{i,n} + w_{i+1,1}}$. Now this collection of basis is normalized orthogonal in the entire radial space. The wave function can be expressed on the basis of them. The vector formed by the coefficients of various bases is what is really recorded in the program.

It is necessary to talk about the boundary condition of the wave function, especially the boundary condition at $r = 0$. As mentioned above, either the Gauss-Lobatto quadrature or the Gauss-Radau quadrature can be used for the outermost finite elements. If the Gauss-Radau quadrature without the left end point is used for the first element, the points x_j do not include -1 : this corresponds to the free boundary condition at $r = 0$. Whereas, the boundary condition is fixed if the Gauss-Lobatto quadrature is applied for the first element. The value of the point $x_1 = -1$ should be given from the physical standpoint. It is generally known that for the SE the boundary condition at $r = 0$ is $\chi(0) = 0$ [33] for the Coulomb potential. Therefore, the value of the left end point is set to 0 in the usual TDSE. This indicates the vector starts at the coefficient of $f_{1,2}$ in our practical calculation. The boundary condition at $r = r_{\text{max}}$ is not so important in our problem, which can simply be set to 0.

Aside from the inner product of wave function, the bilinear form that includes an operator $\langle \psi_j | \hat{O} | \psi_i \rangle$ is frequently used in the calculation. As we just mentioned, the wave function is represented as a vector in the program. Accordingly, an operator can be expressed as a matrix. The simplest operator is the potential operator, which is a diagonal matrix. There also exist some nondiagonal operators, for example, the light-matter interaction operator $\mathbf{p} \cdot \mathbf{A}$ in the velocity gauge. If the polarization direction of the vector potential is along the z axis, the operator can be written as $-iA\nabla_z$ in the dipole approximation. The partial derivative operator acts both on the radial part and the azimuthal part of the wave function

$$\begin{aligned} & \langle \psi'_{\ell'm'} | -iA\nabla_z | \psi_{\ell m} \rangle \\ &= -iA \int \frac{\chi_{\ell m}^*(r)}{r} Y_{\ell'm'}^*(\hat{\mathbf{r}}) \frac{\partial}{\partial z} \frac{\chi_{\ell m}(r)}{r} Y_{\ell m}(\hat{\mathbf{r}}) d^3\mathbf{r} \\ &= -iA \left\{ \sqrt{\frac{\ell^2 - m^2}{(2\ell - 1)(2\ell + 1)}} \delta_{\ell',\ell-1} \delta_{m',m} \right. \\ & \quad \times \int dr \left[\chi_{\ell'm'}^*(r) \frac{\partial \chi_{\ell m}(r)}{\partial r} + \ell \frac{\chi_{\ell'm'}^*(r) \chi_{\ell m}(r)}{r} \right] \\ & \quad + \sqrt{\frac{(\ell + 1)^2 - m^2}{(2\ell + 1)(2\ell + 3)}} \delta_{\ell',\ell+1} \delta_{m',m} \\ & \quad \left. \times \int dr \left[\chi_{\ell'm'}^*(r) \frac{\partial \chi_{\ell m}(r)}{\partial r} - (\ell + 1) \frac{\chi_{\ell'm'}^*(r) \chi_{\ell m}(r)}{r} \right] \right\}. \end{aligned} \tag{A12}$$

The integral about the radial derivative $\chi_{\ell'm'}^*(r) \partial \chi_{\ell m}(r) / \partial r$ is represented by a matrix D . In the finite elements of the Gauss-Lobatto quadrature, the matrix element $D_{j,j'}^i$ can be evaluated by the Gauss quadrature [83]

$$D_{j,j'}^i = \int_{r_i}^{r_{i+1}} f_{i,j} \frac{d}{dr} f_{i,j'} = \begin{cases} \frac{(-1)^{j-j'}}{r_{i,j} - r_{i,j'}}, & j \neq j' \\ \frac{\delta_{j,n} - \delta_{j,1}}{2w_{i,j}}, & j = j'. \end{cases} \tag{A13}$$

Considering the bridge function, the matrix's upper-left and lower-right elements will be canceled out by the neighboring finite element, resulting in an anti-Hermitian matrix in the end. But if the Gauss-Radau quadrature is employed in the first finite element, the matrix of the first derivative D^R is not anti-Hermitian:

$$D_{j,j'}^R = \int_{r_1}^{r_2} f_{1,j} \frac{d}{dr} f_{2,j'} = \begin{cases} \sqrt{\frac{r_j}{r_j'}} \frac{(-1)^{j-j'}}{r_{1,j} - r_{1,j'}}, & j \neq j' \\ \frac{\delta_{j,n}}{w_{1,j}} - \frac{1}{r_{1,j}}, & j = j'. \end{cases} \tag{A14}$$

However, the following operator D^{RA} is anti-Hermitian:

$$D_{j,j'}^{RA} = \int_{r_1}^{r_2} f_{1,j} \frac{d}{dr} \frac{\sqrt{r}}{\sqrt{r_j'}} f_{2,j'} = \begin{cases} \frac{(-1)^{j-j'}}{r_{1,j} - r_{1,j'}}, & j \neq j' \\ \frac{\delta_{j,n}}{2w_{1,j}} r_{1,j}, & j = j'. \end{cases} \tag{A15}$$

It can be utilized to approximate the first derivative [83].

Another common nondiagonal operator is the kinetic operator; the bilinear form with the kinetic operator in the spherical coordinate can be written as

$$\begin{aligned} \langle \psi'_{\ell'm'} | \frac{p^2}{2} | \psi_{\ell m} \rangle &= -\frac{1}{2} \int \left[\chi_{\ell'm'}^*(r) \frac{1}{r} \frac{d}{dr} r^2 \frac{d}{dr} \frac{1}{r} \chi_{\ell m}(r) \right. \\ & \quad \left. - \ell(\ell + 1) \frac{\chi_{\ell'm'}^*(r) \chi_{\ell m}(r)}{r^2} \right] dr. \end{aligned} \tag{A16}$$

The first part is the radial kinetic energy and the other part is the centrifugal potential. If the boundary condition $\chi(0) = 0$ is used, the radial kinetic energy can be reduced to

$$\begin{aligned} & \int \chi_{\ell'm'}^*(r) \frac{1}{r} \frac{d}{dr} r^2 \frac{d}{dr} \frac{1}{r} \chi_{\ell m}(r) dr \\ &= \int \chi_{\ell'm'}^*(r) \frac{d^2}{dr^2} \chi_{\ell m}(r) dr. \end{aligned} \tag{A17}$$

For the right part of Eq. (A17), one can benefit from the integration by parts and the zero boundary condition to express the matrix of the second derivative by the matrix of the first derivative [18]. It is possible to write the kinetic energy matrix $T_{j,j'}^i$ as

$$T_{j,j'}^i = \frac{1}{2} D_{j,k}^i D_{k,j'}^i \tag{A18}$$

in the Gauss-Lobatto quadrature. Whereas, in the Gauss-Radau quadrature, the basis functions are not zero at the left end point. So Eq. (A17) does not hold numerically and the corresponding matrix $T_{j,j'}^R$ should be expressed in its original form

$$T_{j,j'}^R = \frac{1}{2} \left(\frac{1}{r} \right)_{j,j} D_{j,k}^R (r^2)_{k,k} D_{k,j'}^R \left(\frac{1}{r} \right)_{j',j'} \tag{A19}$$

in which the first derivative operator D^R has been given by Eq. (A14). Equations (A19) and (A18) are only expressions in a finite element. Actually, it has been proven that the bilinear form with the kinetic energy operator in the whole range simply equals the sum of that in each element [18]. Therefore, in the actual calculation, both matrices of the first and second derivatives have the form of

$$M = \begin{bmatrix} M_{2,2} & \cdots & M_{2,n-1} & 0 & 0 & \cdots \\ \vdots & \ddots & \vdots & 0 & 0 & \cdots \\ M_{n-1,2} & \cdots & M_{n-1,n-1} & \cdots & M_{n-1,2n-2} & \cdots \\ 0 & 0 & \vdots & \ddots & \vdots & \cdots \\ 0 & 0 & M_{2n-2,n-1} & \cdots & M_{2n-2,2n-2} & \cdots \\ \vdots & \vdots & \vdots & \vdots & \vdots & \ddots \end{bmatrix}.$$

It is clear that the whole matrix is made up of many end-to-end blocks. Each block represents the matrix in a finite element. The outermost elements in each block are related to the bridge function. Additionally, the product of matrices of low-order derivatives can be used to build higher-order derivative matrices, which we mention it in the main text.

APPENDIX B: PROOF OF THE RELATION FOR EIGENSTATES BETWEEN KGE AND SKGE

For a time-independent potential with the spherical symmetry, the KGE can be written as

$$[E_{\text{KG}} - V(r)]^2 \psi_{\text{KG}} = (p^2 c^2 + m_0^2 c^4) \psi_{\text{KG}}. \quad (\text{B1})$$

Whereas the expression of the SKGE is

$$[E_S - V(r)] \psi_S = \sqrt{p^2 c^2 + m_0^2 c^4} \psi_S. \quad (\text{B2})$$

The inner product of two eigenstates is written as $\langle \psi_{\text{KG}2} | \frac{E_1 - V(r) + E_2 - V(r)}{2m_0 c^2} | \psi_{\text{KG}1} \rangle$ for the KGE, whereas it is $\langle \psi_{S2} | \psi_{S1} \rangle$ for the SKGE. It is easy to guess that $\psi_S = \sqrt{\frac{[E - V(r)]}{m_0 c^2}} \psi_{\text{KG}}$ may be a good approximation up to the first-order relativistic correction. This speculation will be demonstrated in the following.

Let us consider a weak relativistic situation, in which the potential and kinetic energy are both much smaller than the rest mass, i.e., $|V(r)| \ll m_0 c^2$ and $p^2/2m_0 \ll m_0 c^2$, respectively. The eigenstates and eigenvalues of the two equations are assumed to be expanded in a series of $1/c^2$:

$$\begin{aligned} E &= m_0 c^2 + E^{(0)} + E^{(1)} + \cdots, \\ \psi &= \psi^{(0)} + \psi^{(1)} + \cdots. \end{aligned} \quad (\text{B3})$$

First of all, we rewrite two equations as functions of $E - m_0 c^2$:

$$\begin{aligned} [E_{\text{KG}} - m_0 c^2 - V(r)] \left[1 + \frac{E_{\text{KG}} - m_0 c^2 - V(r)}{2m_0 c^2} \right] \psi_{\text{KG}} \\ = \frac{p^2}{2m_0} \psi_{\text{KG}}, \\ [E_S - m_0 c^2 - V(r)] \psi_S = (\sqrt{p^2 c^2 + m_0^2 c^4} - m_0 c^2) \psi_S. \end{aligned} \quad (\text{B4})$$

The zero-order expansions of equations are

$$\begin{aligned} [E_{\text{KG}}^{(0)} - m_0 c^2 - V(r)] \psi_{\text{KG}}^{(0)} &= \frac{p^2}{2m_0} \psi_{\text{KG}}^{(0)}, \\ [E_S^{(0)} - m_0 c^2 - V(r)] \psi_S^{(0)} &= \frac{p^2}{2m_0} \psi_S^{(0)}. \end{aligned} \quad (\text{B5})$$

Both of them should deduce to the SE, so $E_{\text{KG}}^{(0)} = E_S^{(0)}$ and $\psi_{\text{KG}}^{(0)} = \psi_S^{(0)}$. And then we can write the first-order expansions for the two equations

$$\begin{aligned} [E_{\text{KG}}^{(0)} - m_0 c^2 - V(r)] \psi_{\text{KG}}^{(1)} + \frac{[E_{\text{KG}}^{(0)} - m_0 c^2 - V(r)]^2}{2m_0 c^2} \psi_{\text{KG}}^{(0)} \\ + E_{\text{KG}}^{(1)} \psi_{\text{KG}}^{(0)} = \frac{p^2}{2m_0} \psi_{\text{KG}}^{(1)}, \\ [E_S^{(0)} - m_0 c^2 - V(r)] \psi_S^{(1)} + E_S^{(1)} \psi_S^{(0)} \\ = \frac{p^2}{2m_0} \psi_S^{(1)} - \frac{p^4}{8m_0^3 c^2} \psi_S^{(0)}. \end{aligned} \quad (\text{B6})$$

It is easy to note that first-order corrections of eigenvalues are the same for two equations:

$$E_{\text{KG}}^{(1)} = \langle \psi_{\text{KG}}^{(0)} | - \frac{[E_{\text{KG}}^{(0)} - m_0 c^2 - V(r)]^2}{2m_0 c^2} | \psi_{\text{KG}}^{(0)} \rangle = E_S^{(1)} = \langle \psi_S^{(0)} | - \frac{p^4}{8m_0^3 c^2} | \psi_S^{(0)} \rangle. \quad (\text{B7})$$

Next, the first-order expansion of the SKGE will be transformed as following:

$$\begin{aligned} [E_S^{(0)} - m_0 c^2 - V(r)] \psi_S^{(1)} + E_S^{(1)} \psi_S^{(0)} &= \frac{p^2}{2m_0} \psi_S^{(1)} - \frac{p^4}{8m_0^3 c^2} \psi_S^{(0)}, \\ [E_S^{(0)} - m_0 c^2 - V(r)] \psi_S^{(1)} + E_S^{(1)} \psi_S^{(0)} &= \frac{p^2}{2m_0} \psi_S^{(1)} - \frac{p^2}{4m_0^2 c^2} [E_S^{(0)} - m_0 c^2 - V(r)] \psi_S^{(0)}, \end{aligned}$$

$$\begin{aligned}
& [E_S^{(0)} - m_0c^2 - V(r)]\psi_S^{(1)} + E_S^{(1)}\psi_S^{(0)} = \frac{p^2}{2m_0} \left\{ \psi_S^{(1)} - \frac{[E_S^{(0)} - m_0c^2 - V(r)]}{2m_0c^2} \psi_S^{(0)} \right\}, \\
& [E_S^{(0)} - m_0c^2 - V(r)] \left\{ \psi_S^{(1)} - \frac{[E_S^{(0)} - m_0c^2 - V(r)]}{2m_0c^2} \psi_S^{(0)} \right\} + \frac{[E_S^{(0)} - m_0c^2 - V(r)]^2}{2m_0c^2} \psi_S^{(0)} \\
& + E_S^{(1)}\psi_S^{(0)} = \frac{p^2}{2m_0} \left\{ \psi_S^{(1)} - \frac{[E_S^{(0)} - m_0c^2 - V(r)]}{2m_0c^2} \psi_S^{(0)} \right\}, \\
& [E_{\text{KG}}^{(0)} - m_0c^2 - V(r)] \left\{ \psi_S^{(1)} - \frac{[E_{\text{KG}}^{(0)} - m_0c^2 - V(r)]}{2m_0c^2} \psi_{\text{KG}}^{(0)} \right\} \\
& + \frac{[E_{\text{KG}}^{(0)} - m_0c^2 - V(r)]^2}{2m_0c^2} \psi_{\text{KG}}^{(0)} + E_{\text{KG}}^{(1)}\psi_{\text{KG}}^{(0)} = \frac{p^2}{2m_0} \left\{ \psi_S^{(1)} - \frac{[E_{\text{KG}}^{(0)} - m_0c^2 - V(r)]}{2m_0c^2} \psi_{\text{KG}}^{(0)} \right\}. \tag{B8}
\end{aligned}$$

We can get $\psi_S^{(1)} - \frac{[E_{\text{KG}}^{(0)} - m_0c^2 - V(r)]}{2m_0c^2} \psi_{\text{KG}}^{(0)} = \psi_{\text{KG}}^{(1)}$ by comparing the last equation to the first-order expansion of KGE (B6). It is equivalent to $\psi_S = \sqrt{\frac{[E - V(r)]}{m_0c^2}} \psi_{\text{KG}}$ up to the first order, which is our expectation.

The conclusion is that SKGE has the same eigenvalues and eigenstates (after considering different inner product forms) with the KGE up to the first relativistic correction. The consistency can be easily extended to any observable for the first-order relativistic correction as shown in the main text.

-
- [1] J. Sucher, *J. Math. Phys.* **4**, 17 (1963).
[2] W. Lucha, F. F. Schöberl, and D. Gromes, *Phys. Rep.* **200**, 127 (1991).
[3] W. Lucha and F. F. Schöberl, *Int. J. Mod. Phys. A* **14**, 2309 (1999).
[4] T. K. Lindblom, M. Førre, E. Lindroth, and S. Selstø, *Phys. Rev. Lett.* **121**, 253202 (2018).
[5] W. Greiner, *Relativistic Quantum Mechanics*, Vol. 2 (Springer, Berlin, 2000).
[6] S. Selstø, E. Lindroth, and J. Bengtsson, *Phys. Rev. A* **79**, 043418 (2009).
[7] Y. V. Vanne and A. Saenz, *Phys. Rev. A* **85**, 033411 (2012).
[8] I. A. Ivanov, *Phys. Rev. A* **91**, 043410 (2015).
[9] D. A. Telnov and S.-I. Chu, *Phys. Rev. A* **102**, 063109 (2020).
[10] M. Ruf, H. Bauke, and C. H. Keitel, *J. Comput. Phys.* **228**, 9092 (2009).
[11] H. Bauke, H. G. Hetzheim, G. R. Mocken, M. Ruf, and C. H. Keitel, *Phys. Rev. A* **83**, 063414 (2011).
[12] M. Ruf, G. R. Mocken, C. Müller, K. Z. Hatsagortsyan, and C. H. Keitel, *Phys. Rev. Lett.* **102**, 080402 (2009).
[13] R. Taïeb, V. Véniard, and A. Maquet, *Phys. Rev. Lett.* **81**, 2882 (1998).
[14] S. Hu, A. F. Starace, W. Becker, W. Sandner, and D. Milosevic, *J. Phys. B: At., Mol. Opt. Phys.* **35**, 627 (2002).
[15] M. Førre, *Phys. Rev. A* **99**, 053410 (2019).
[16] M. Førre and S. Selstø, *Phys. Rev. A* **101**, 063416 (2020).
[17] A. Gordon, R. Santra, and F. X. Kärtner, *Phys. Rev. A* **72**, 063411 (2005).
[18] T. N. Rescigno and C. W. McCurdy, *Phys. Rev. A* **62**, 032706 (2000).
[19] F. Blumenthal and H. Bauke, *J. Comput. Phys.* **231**, 454 (2012).
[20] J. J. Sakurai, *Advanced Quantum Mechanics* (Pearson Education, London, 2006).
[21] H. Feshbach and F. Villars, *Rev. Mod. Phys.* **30**, 24 (1958).
[22] A. Mostafazadeh, *Classical Quantum Gravity* **20**, 155 (2003).
[23] A. Mostafazadeh and F. Zamani, *Ann. Phys.* **321**, 2183 (2006).
[24] A. Mostafazadeh, *Int. J. Geom. Methods Mod. Phys.* **07**, 1191 (2010).
[25] D. Calvetti, L. Reichel, and D. C. Sorensen, *Electron. Trans. Numer. Anal.* **2**, 21 (1994).
[26] L. Lehtovaara, J. Toivanen, and J. Eloranta, *J. Comput. Phys.* **221**, 148 (2007).
[27] W. Gautschi, *SIAM Rev.* **9**, 24 (1967).
[28] L.-Y. Peng and Q. Gong, *Comput. Phys. Commun.* **181**, 2098 (2010).
[29] G. Hadinger, M. Aubert-Frécon, and G. Hadinger, *J. Phys. B: At., Mol. Opt. Phys.* **29**, 2951 (1996).
[30] X.-F. Hou, L.-Y. Peng, Q.-C. Ning, and Q. Gong, *J. Phys. B: At., Mol. Opt. Phys.* **45**, 074019 (2012).
[31] M. Førre and A. S. Simonsen, *Phys. Rev. A* **90**, 053411 (2014).
[32] E. Anderson, Z. Bai, C. Bischof, L. S. Blackford, J. Demmel, J. Dongarra, J. Du Croz, A. Greenbaum, S. Hammarling, A. McKenney *et al.*, *LAPACK Users' guide* (SIAM, Philadelphia, 1999).
[33] L. D. Landau and E. M. Lifshitz, *Quantum Mechanics: Non-relativistic Theory*, Vol. 3 (Elsevier, Amsterdam, 2013).
[34] H. M. Pilkuhn, *Relativistic Particle Physics* (Springer, New York, 2013).
[35] A. Barnett, *Comput. Phys. Commun.* **24**, 141 (1981).
[36] A. F. Starace, in *Theory of Atomic Photoionization*, Handbuch der Physik Vol. 31 (Springer-Verlag, Berlin, 1982), pp. 1–121.
[37] J. Liesen and Z. Strakos, *Krylov Subspace Methods: Principles and Analysis* (Oxford University Press, Oxford, 2013).
[38] M. Hochbruck and C. Lubich, *SIAM J. Numer. Anal.* **34**, 1911 (1997).
[39] S. Wang and W.-C. Jiang, *Chin. Phys. B* **31**, 013201 (2022).
[40] Z. Bai, J. Demmel, J. Dongarra, A. Ruhe, and H. van der Vorst, *Templates for the Solution of Algebraic Eigenvalue Problems: A Practical Guide* (SIAM, Philadelphia, 2000).

- [41] R. B. Lehoucq, D. C. Sorensen, and C. Yang, *ARPACK Users' Guide: Solution of Large-scale Eigenvalue Problems with Implicitly Restarted Arnoldi Methods* (SIAM, Philadelphia, 1998).
- [42] T. L. Gill and W. Zachary, *J. Phys. A: Math. Gen.* **38**, 2479 (2005).
- [43] C. Lämmerzahl, *J. Math. Phys.* **34**, 3918 (1993).
- [44] A. Torre, A. Lattanzi, and D. Levi, *Ann. Phys.* **529**, 1600231 (2017).
- [45] M. Vogl, P. Laurell, H. Zhang, S. Okamoto, and G. A. Fiete, *Phys. Rev. Res.* **2**, 043243 (2020).
- [46] G. Dattoli, E. Sabia, K. Górska, A. Horzela, and K. Penson, *J. Phys. A: Math. Theor.* **48**, 125203 (2015).
- [47] I. W. Herbst, *Commun. Math. Phys.* **53**, 285 (1977).
- [48] N. Brambilla and A. Vairo, *Phys. Lett. B* **359**, 133 (1995).
- [49] A. Leyaouanc, L. Oliver, and J. Raynal, *Ann. Phys.* **239**, 243 (1995).
- [50] B. Durand and L. Durand, *Phys. Rev. D* **28**, 396 (1983).
- [51] C. Semay, D. Baye, M. Hesse, and B. Silvestre-Brac, *Phys. Rev. E* **64**, 016703 (2001).
- [52] A. Wachter, *Relativistic Quantum Mechanics* (Springer, Berlin, 2011).
- [53] Y. Huang, Y. Jia, and R. Yu, [arXiv:1812.11957](https://arxiv.org/abs/1812.11957).
- [54] A. D. Bandrauk and H. Shen, *Chem. Phys. Lett.* **176**, 428 (1991).
- [55] C. Leforestier, R. Bisseling, C. Cerjan, M. Feit, R. Friesner, A. Guldberg, A. Hammerich, G. Jolicard, W. Karrlein, H.-D. Meyer *et al.*, *J. Comput. Phys.* **94**, 59 (1991).
- [56] W.-C. Jiang and X.-Q. Tian, *Opt. Express* **25**, 26832 (2017).
- [57] F. Fillion-Gourdeau, E. Lorin, and A. D. Bandrauk, *Comput. Phys. Commun.* **183**, 1403 (2012).
- [58] T. Kjellsson, Relativistic light-matter interaction, Ph.D. thesis, Department of Physics, Stockholm University, 2015.
- [59] J. Naudts, [arXiv:physics/0507193](https://arxiv.org/abs/physics/0507193).
- [60] A. I. Nikishov and V. I. Ritus, *Zh. Éksp. Teor. Fiz.* **50**, 255 (1966) [*Sov. Phys. JETP* **23**, 255, 1966].
- [61] N. Milosevic, V. P. Krainov, and T. Brabec, *J. Phys. B: At., Mol. Opt. Phys.* **35**, 3515 (2002).
- [62] C. J. Joachain and N. J. Kylstra, *Phys. Rev. A* **100**, 013417 (2019).
- [63] M. Klaiber, E. Yakaboylu, H. Bauke, K. Z. Hatsagortsyan, and C. H. Keitel, *Phys. Rev. Lett.* **110**, 153004 (2013).
- [64] M. Lewenstein, P. Balcou, M. Y. Ivanov, A. L'Huillier, and P. B. Corkum, *Phys. Rev. A* **49**, 2117 (1994).
- [65] C. C. Chirilă, C. J. Joachain, N. J. Kylstra, and R. M. Potvliege, *Phys. Rev. Lett.* **93**, 243603 (2004).
- [66] M. Klaiber, K. Z. Hatsagortsyan, and C. H. Keitel, *Phys. Rev. A* **75**, 063413 (2007).
- [67] H. K. Avetissian, A. G. Markossian, and G. F. Mkrtchian, *Phys. Rev. A* **84**, 013418 (2011).
- [68] S. X. Hu and C. H. Keitel, *Phys. Rev. A* **63**, 053402 (2001).
- [69] J. C. Baggesen and L. B. Madsen, *J. Phys. B: At., Mol. Opt. Phys.* **44**, 115601 (2011).
- [70] G. W. Stewart, *SIAM J. Matrix Anal. Appl.* **23**, 601 (2002).
- [71] C. K. Dumlu and G. V. Dunne, *Phys. Rev. D* **83**, 065028 (2011).
- [72] C. Fey and R. Schützhold, *Phys. Rev. D* **85**, 025004 (2012).
- [73] S. Villalba-Chávez and C. Müller, *Phys. Lett. B* **718**, 992 (2013).
- [74] A. I. Titov, H. Takabe, and B. Kämpfer, *Phys. Rev. D* **98**, 036022 (2018).
- [75] G. Baur, K. Hencken, and D. Trautmann, *Phys. Rep.* **453**, 1 (2007).
- [76] Q. Z. Lv, H. Bauke, Q. Su, C. H. Keitel, and R. Grobe, *Phys. Rev. A* **93**, 012119 (2016).
- [77] G. R. Mocken, M. Ruf, C. Müller, and C. H. Keitel, *Phys. Rev. A* **81**, 022122 (2010).
- [78] C. Müller, C. Deneke, and C. H. Keitel, *Phys. Rev. Lett.* **101**, 060402 (2008).
- [79] C. Müller, A. B. Voitkiv, and N. Grün, *Phys. Rev. Lett.* **91**, 223601 (2003).
- [80] C. Müller, A. B. Voitkiv, and N. Grün, *Phys. Rev. A* **67**, 063407 (2003).
- [81] C. Müller, A. B. Voitkiv, and N. Grün, *Phys. Rev. A* **70**, 023412 (2004).
- [82] H. Michels, *Math. Comp.* **17**, 237 (1963).
- [83] H. Liang, X.-R. Xiao, Q. Gong, and L.-Y. Peng, *J. Phys. B: At., Mol. Opt. Phys.* **50**, 174002 (2017).